Impact of a new emission inventory on CAM5 simulations of aerosols and aerosol radiative effects in eastern China

Tianyi Fan[1], Xiaohong Liu[1,2], Po-Lun Ma[3], Qiang Zhang[4], Zhanqing Li[1, 5], Yiquan Jiang[6], Fang Zhang[1], Chuanfeng Zhao[1], Xin Yang[1]

[1]College of Global Change and Earth System Science, and State Key Laboratory of Earth Surface Processes and Resource Ecology, Beijing Normal University, Beijing, China
[2]Department of Atmospheric Science, University of Wyoming, Laramie, Wyoming, USA
[3]Atmospheric Sciences and Global Change Division, Pacific Northwest National Laboratory, Richland, Washington, USA
[4]Center for Earth System Science, Tsinghua University, Beijing, China
[5]Department of Atmospheric and Oceanic Science & ESSIC, University of Maryland, College Park, Maryland, USA
[6]Institute for Climate and Global Change Research, School of Atmospheric Sciences, Nanjing University, Nanjing, China

Correspondence to: Tianyi Fan (fantianyi@bnu.edu.cn)

Abstract. Emissions of aerosols and gas precursors in China have increased significantly over the past three decades with the rapid economic growth. These increases might have a large climate effect. However, global aerosol-climate models often show large biases in aerosol distribution and radiative forcing in China, and these biases are often attributed to uncertainties and biases associated with the emission inventory used to drive the models. In this study, an energy-statics and technology-based emission inventory, Multi-scale Emission Inventory for China (MEIC), was compiled and used to drive the Community Atmosphere Model Version 5 (CAM5) to evaluate aerosol distribution and radiative effects in China against observations, compared with the model simulations with the widely-used IPCC AR5 emission inventory. We found that the new MEIC emission improves the annual mean AOD simulations in eastern China by 12.9% compared with MODIS observations and 14.7% compared with MISR observations, and explains 22%-28% of the AOD low bias simulated with the AR5 emission. Seasonal variation of the MEIC emission leads to a better agreement with the observed surface concentrations of primary aerosols (i.e., primary organic carbon and black carbon) than the AR5 emission, while the seasonal variation of secondary aerosols (i.e., sulfate and secondary organic aerosol) depends less on the emission. The new emission inventory estimates the annual averaged aerosol direct radiative effect at TOA, surface, and atmosphere to be -0.50, -12.76, and 12.26 W m^{-2} respectively over eastern China, which are enhanced by -0.19, -2.42, and 2.23 W m^{-2} compared with the AR5 emission. Due to higher winter BC emission in MEIC, the atmospheric warming effect and the surface cooling of BC are twice as much as those using the AR5 emission. This study highlights the importance of improving the aerosol and gas precursor emissions in modeling the atmospheric aerosols and their radiative effects.

Keywords: Emission inventory in China; Aerosol; Aerosol radiative effects; CAM5

1 Introduction

China has been experiencing three decades of rapid economic growth that brings emissions of atmospheric pollutants that are very different from the past and other parts of the world (Streets et al., 2008; Zhang et al., 2009; Klimont et al., 2009; Lu et al., 2010; Lei et al., 2011; Wang et al., 2012). In 2000, the emissions of sulfur dioxide (SO_2), black carbon (BC), and organic carbon (OC) in eastern China accounted for 18.8%, 17.3% and 8.7% of global total emissions, respectively (Liao et al., 2015). China's relative contribution to the global radiative forcing due to emission of sulfate, nitrate, BC, and OC are estimated to be 28%, 24%, 14%, and 5%, respectively (Li et al., 2016).

Emissions of aerosols and their precursor gases in East Asia remain highly uncertain (Zhao et al., 2011; Fu et al., 2012; Wang et al., 2014; Chang et al., 2015; Zhang et al., 2015). The uncertainties (defined as 95% confidence intervals around the central estimates from Monte-Carlo experiments) of a bottom-up Chinese emission are -14% to 13% for SO_2, -13% to 37% for NO_x, -25% to 136% for BC and -40% to 121% for OC (Zhao et al., 2011). Using a different definition of the uncertainty (standard deviation divided by the mean value across different inventories), Chang et al. (2015) estimate that the uncertainties of the surface concentrations of sulfate, nitrate, BC, primary organic matter (POM), and secondary organic aerosol (SOA) due to emissions are 3.9%, 40.0%, 11.1%, 16.7%, and 15.4% over eastern China, respectively.

The uncertainties of emission inventories can affect the model simulations of the aerosols and their radiative effects. Shindell et al. (2013) shows that aerosol optical depth (AOD) are underestimated in East Asia by the multi-model mean of 10 Climate Model Intercomparison Program phase 5 (CMIP5) (Taylor et al., 2012) models compared with satellite observations. Eight out of the 10 global climate models underestimate the AOD by about -36% to -58% relative to ground-based Aerosol Robotic Network (AERONET) observations. The AOD biases are substantially larger than those in North America and Europe. For example, the Community Atmospheric Model version 5 (CAM5) significantly underestimates AOD in East Asia (Liu et al., 2012). A moderate emission adjustment (idealized 20%-30% regional increases in SO_2, OC, and BC emissions) largely improves the simulations of precursor gases and primary aerosols from CAM5 (He and Zhang, 2014). To examine the impact of the emission inventory on the simulation of aerosols and their radiative effects in CAM5, it is straightforward to replace the default emission inventory in China with a new one that is supposed to improve the representation of the current status of Chinese emissions of aerosols and gas precursors.

The default emission inventory of CAM5 was prepared following the protocol of the Intergovernmental Panel on Climate Change (IPCC) Fifth Assessment Report (AR5) experiments. In order to provide a consistent emission inventory for the CMIP5 models participating the IPCC AR5, a global historical (1850~2000) dataset for anthropogenic and biomass burning emissions of aerosols and reactive gases was developed (Lamarque et al., 2010). In East Asia the AR5 emission inventory incorporates the Regional Emission inventory in ASia (REAS) dataset (Ohara et al., 2007). The IPCC AR5 emission inventory has been widely used for global and regional climate studies (Giorgi et al., 2009; Jones et al., 2011; Shindell et al., 2013). However, the AR5 emission inventory has disadvantages in modelling the rapid change of aerosols in China. For example, data are updated every 10 years since annual data are available only in recent past and for limited species. Seasonal

variations are ignored for all emissions except biomass burning, soil NO_x, ship and aircraft emissions due to limited data availability.

To characterize the rapid change of China's emissions, an improved technology-based Multi-scale Emission Inventory for China (MEIC) is developed at Tshinghua University, China (http://www.meicmodel.org/index.html). MEIC covers 10 major atmospheric pollutants and over 700 anthropogenic emission sources from 1990 to 2012. It has the following advantages compared with the AR5 emission inventory: (1) adoption of a detailed technology-based approach, (2) application of a dynamic methodology of rapid technology renewal, (3) re-examination of China's energy statistics, and (4) monthly emissions to represent species that have strong seasonal variations for the model results to be better compared with time-specific measurements (Zhang et al*.,* 2009). The MEIC emission inventory is verified to produce consistent aerosol precursor loadings with satellite observations (Li et al., 2010; Wang et al., 2010, 2012; Zhang et al., 2012; Liu et al., 2016). It has widely been used to study the trend of aerosol concentrations in China (Wang et al., 2013), the Asian air pollution outflow (Zhang et al., 2008; Chen et al., 2009), relative contribution of emission and meteorology to the aerosol variability (Xing et al., 2011) and sensitivity of air quality to precursor emissions (Liu et al., 2010).

Here we examine the impacts on aerosol concentrations and their radiative effects simulated from CAM5 due to the change of emission datasets from the default AR5 to the new MEIC emission inventory. With the inclusion of emission seasonality in MEIC, we will be able to isolate the seasonal variation of aerosol concentrations due to the impact of meteorological factors (*e.g.,* temperature, precipitation, wind speed, etc.) from the impact of emission seasonality. For example, monsoon precipitation induces seasonal shift of the spatial distribution of AOD over eastern China without including the seasonal variation of the aerosol emissions (Jiang et al., 2015).

We rely on climate models to estimate the historical and future change of aerosol direct radiative effect (ADRE). However, the uncertainty of aerosol emissions used in the climate models could add another dimension of uncertainty in simulating the change of aerosol radiative effect. The emission structure changed in China during the last decade. The emission of SO_2 decreased by 9.2% from 34.0 Tg in 2006 to 30.8 Tg in 2010 (-2.4% annual growth rate) (Lu et al., 2011). The NH_3 emission decreased slightly from 10.5 Tg in 2006 to 9.7 Tg in 2012 with an annual rate of -1.4% (Kang et al., 2016). Meanwhile, some researches show that the emissions of BC, OC, and NO_x have been increasing since 2006. The BC/OC emissions increase from 1.6 Tg/3.6Tg in 2004 to 1.9 Tg/4.0 Tg in 2010, with an annual growth rate of 2.8%/1.7%. The MEIC developer team estimates that the emission of BC/OC decreased from 2006 to 2010 due to reduced emissions in the domestic and transportation sectors. The NO_x emission grew by 113.9% from 12.2 Tg in 2000 to 26.1 Tg in 2010, with an annual growth rate of 7.9% (Zhao et al., 2010). To examine the change in the ADRE as the change in the emission structure, we also carry out a simulation using MEIC emission from 2002 to 2012.

This paper is organized as follows. Sect. 2 describes the model configurations and how MEIC is incorporated in the model. Sect. 3 shows the results of aerosol properties and their radiative effects simulated from the model using the new MEIC emission compared to the AR5 emission. Sect. 4 discusses the change of aerosol radiative effects over eastern China as the change of emission uncertainty in the last decade. Conclusions are presented in Sect. 5.

2 Method

2.1 Model configuration

We run the simulations with the National Center for Atmospheric Research (NCAR) CAM5 with the 3-mode Modal Aerosol Model (MAM3), which represents aerosol size distribution and mixing state between aerosol components in the Aitken, accumulation, and coarse modes (Liu et al., 2012). The aerosol species include sulfate, BC, POM, SOA, dust, and sea salt. MAM3 assumes that the aerosol species are internally mixed within modes and externally mixed among modes. The mass mixing ratio of each aerosol species in the mode and the number mixing ratio of the mode are predicted. The emission, transport, gas- and aqueous-phase chemical production, dry and wet deposition, microphysics (nucleation, condensation and coagulation), and physical, chemical and optical properties of aerosol are simulated in a physically based manner. The transported gas species are SO_2, H_2O_2, dimethyl-sulfide (DMS), H_2SO_4 and a lumped semi-volatile organic gas species (SOAG). The aerosol radiative effects are calculated in CAM5 with the Rapid Radiative Transfer Model for GCMs (RRTMG) (Iacono et al., 2008). The refractive indices for most aerosol components are taken from OPAC (Hess et al., 1998), but for BC the value (1.95, 0.79i) from Bond and Bergstrom (2006) is used.

We run CAM5 in a "constrained meteorology" mode where the model meteorological fields (winds, temperatures, etc.) are nudged towards ERA-Interim (Dee et al., 2011) with 6 h relaxation timescale (Ma et al., 2013, 2014; Zhang et al., 2014). The constrained meteorology technique facilitates the model-observation comparison of aerosols and gas species. When simulating the decadal change from 2002 to 2012, we use the reanalysis data in 2009 cyclically to nudge the model meteorological fields. In this way, the change of aerosol concentration is controlled by the change of emission alone since the meteorological fields are identical among the years.

The horizontal resolution is $0.9^o \times 1.25^o$ and vertically there are 30 layers from surface to 2.25 hPa, with the lowest 4 layers inside the boundary layer. We focus our analysis of model results over eastern China (22^o-44^oN, 100^o-124^oE, the red frame in Fig. 1) where the active anthropogenic emissions are located.

2.2 Mapping the MEIC emission inventory for CAM5

In addition to running CAM5 with the default AR5 emission inventory, we implement the new emission inventory MEIC into the model. We replace the default AR5 emission with the MEIC emission in China and keep the same as the AR5 emission elsewhere. We process the MEIC emission in the same way as the AR5 emission is processed for the CAM5 simulations. We map the MEIC aerosols and precursor gases in different sectors to those required by the CAM5 chemistry and aerosol modules (see Table S1 in the supplementary materials). MEIC includes anthropogenic emissions in sectors named by power, industry, residential, and transportation, which correspond to the AR5 emission sectors named by energy, industry, domestic, and transportation, respectively. Emissions due to shipping, agricultural waste burning and waste treatment as well as natural sources such as forest fires, grass fires and continuous volcanoes are not specified in the MEIC emission, so we keep them the same as those in the AR5 emission.

MEIC provides the emissions of aerosols and precursor gases including SO_2, BC, OC, and non-methane volatile organic compounds (NMVOCs). Additional work is done to obtain a full set of species required by CAM5-MAM3 aerosol simulations, which includes SO_2, primary sulfate aerosol, BC, POM, SOAG, DMS, and number concentration in the accumulation and Aitken modes. These aerosols and precursor gases are emitted as surface or elevated sources. 2.5% (by molar) of the SO_2 emission is regarded as the primary sulfate aerosol emitted directly from sources following the Aerosol Comparisons between Observations and Models (AeroCom) protocol (Dentener et al., 2006) and the rest are emitted as SO_2. The energy and industrial SO_2 and primary sulfate are treated as elevated sources at 3 levels between 100 and 300 m, and their sources due to forest fires and grass fires are emitted in six vertical levels at 0 to 6 km (Dentener et al., 2006). SO_2 and primary sulfate from agriculture, domestic, transportation, waste, and shipping sectors are emitted at surface. Primary sulfate aerosols from domestic and transportation are put in the Aitken mode and those from other sectors are put in the accumulation mode (Liu et al., 2012).

The POM emission is assumed to be 1.4 times the OC emission in order to include the aerosol mass of other elements (i.e., oxygen, hydrogen, and nitrogen) (Seinfeld and Pandis, 1998). POM and BC from forest fires and grass fires are treated as elevated sources, while POM and BC from other sectors are treated as surface sources. All POM and BC aerosols are put in the accumulation mode. The SOAG species in CAM5-MAM3 are lumped semi-volatile organic gas-phase species that can condense onto pre-existing aerosols to form SOA. Since the IPCC AR5 dataset does not provide biogenic volatile organic compound (VOC) emission, to simulate SOA in CAM5-MAM3, the SOAG emission is derived from the emission fluxes of five primary VOC categories (isoprene, monoterpenes, big alkanes, big alkenes, toluene) that are prescribed from the Model for OZone And Related chemical Tracers version 4 (MOZART-4) dataset (Emmons et al., 2010) In MOZART-4 the biogenic emissions of isoprene and monoterpenes are based on the Model for Emissions of Gases and Aerosols Emissions from Nature (MEGAN) (Guenther et al., 2006). The MEIC emission provides anthropogenic sources of the five VOC categories and the mapping table for lumping the MEIC VOC species to MOZART is provided by Li et al. (2014). Since the MEIC emission inventory does not provide biogenic sources of isoprene and monoterpenes, which are much larger than their anthropogenic sources, we make the total emissions from anthropogenic and natural sources of these two species the same as those in the AR5 emission. To derive the emissions of the SOAG species, the MEIC emissions of the VOCs are multiplied by the assumed mass yields (Liu et al., 2012). We note that the emissions of SOAGs are increased by a factor of 1.5 in CAM5 to account for the large uncertainty in SOA formation.

The number emission fluxes in both AR5 and MEIC are calculated from the mass fluxes in a consistent way. The mass to number conversion is based on $E_{number} = E_{mass} / \left(\frac{\pi}{6} \rho {D_v}^3\right)$, where D_v is the volume-mean emitted diameter and ρ is the aerosol particle density (Liu et al., 2012). Since the MEIC emission does not provide mass emissions from agricultural waste burning, waste treatment, forest fire, grass fire and continuous volcanoes, we use the number fluxes from the AR5 emission for these sectors.

Since the reanalysis data used for our offline meteorology is for year 2009, we obtain the emissions in 2009 by the linear interpolation between year 2008 and 2010 for the MEIC emission and between year 2005 and 2010 for the AR5 emission.

To examine the change in the ADRE as the change in the emission structure, we carry out a simulation using MEIC emission from 2002 to 2012. We choose these 11 years because China's economy recovered from a depression in 2002, and since then the SO_2 emission has started to grow dramatically and decreased after 2006 due to the application of desulfurization equipment. After 2012 the annual emission rates did not change as dramatically as the previous years.

2.3 Aerosol observational data

AOD retrievals from MODIS and MISR in 2009 are used to compare against the model results. This study uses the monthly mean AOD from MODIS Terra collection 6 (MOD08_M3), which were obtained from NASA Level1 and Atmosphere Archive and Distribution System (LAADS, https://ladsweb.nascom.nasa.gov/). We use the combined MODIS AOD retrievals of the Dark Target (Levy et al., 2010) and the Deep Blue (Hsu et al., 2004) algorithms.

The AERONET AOD and single scattering albedo (SSA) retrievals in 12 sites in Mainland China, Hongkong, Taiwan, Japan, and Korea are used to compare with the model results and the locations are shown in Fig. 1. We calculate the monthly averaged AOD and SSA in 2009 from the daily averages and exclude the months with less than 3 daily values.

Chemical observation data of surface concentrations in China are collected from literatures (see Table S2 and the references in the supplementary materials). The chemical compositions of particulate matter with diameter smaller than 2.5 μm ($PM_{2.5}$) are analyzed for sulfate, OC, BC, and SOA in these studies. The measured OC concentrations are multiplied by a factor of 1.4 for calculation of the total organic mass (Seinfeld and Pandis, 1998). To characterize the seasonal cycle of a full year, we extend our time selection of the observations from 2009 to 2010. Many of the studies collected the samples continuously during April, July, October, and January to represent the concentrations in spring, summer, autumn, and winter. The observation in Xiamen was carried out for a full year of sample collection. For the observations that only lasted for several days within a month, we average the daily data to represent the month. Since we do not find the SOA measurements in 2009, we use the data in other years and are aware of the uncertainties due to the time difference. The geographical locations of these chemical observations are shown in Fig. 1.

2.4 Aerosol direct radiative effect calculation and observational data

We estimate the ADRE due to instantaneous impact of aerosol scattering and absorption on the Earth's energy budget in 2009 following the method by Ghan (2013). The ADRE is calculated by the difference between the "all-sky" radiative flux in the standard model simulation and a diagnostic call to the model radiation code from the same simulation but neglecting the aerosol scattering and absorption. This method considers the impact of cloud presence on the aerosol ADRE, which is different than the conventional method that considers the clear-sky flux changes only (references in Ghan, 2013). The advantage is that this method takes into account the radiative warming enhanced by absorbing aerosol above clouds. We

calculate the shortwave ADREs of all aerosols and each individual aerosol species (sulfate, BC, POM, SOA) at the top of the atmosphere (TOA), at the surface, and in the atmosphere.

The ADREs have been estimated based on ground-based and satellite observations at different locations in China (*Li et al.,* 2016). Table S3 in the supplementary materials lists the observations used in this study. Most of the data are from the Chinese Sun Hazemeter Network (CSHNET) (Xin et al., 2007; Li et al., 2010). The ADREs are consistently defined as difference of the irradiance at TOA, surface, and in the atmosphere with and without the presents of aerosols. The ADREs are either calculated by radiative transfer models using the measured or retrieved aerosol properties (AOD, single scattering albedo (SSA), phase function, Ångström exponent (AE), and size distribution) and surface reflectance (Xia et al., 2007a; Li et al., 2010; Liu et al., 2011; Zhuang et al., 2014), or derived from the fitting equation of irradiance measurements as a function of AOD (Xia et al., 2007b, c). Since the MEIC emission inventory is for anthropogenic aerosols, we only compare with observations that are free of the impact of dust aerosol near deserts. For the same reason, the shortwave radiation is discussed since anthropogenic aerosols are mostly fine particles, the impact of which in the long-wave radiation can be ignored. All data analyses are performed after cloud screening to ensure clear-sky conditions. Since the solar irradiance depends on solar zenith angle (i.e., the time of the day), we compare with the measurements that are 24 h averaged. If both the TOA and the surface ADREs are provided, we calculated the ADRE in the atmosphere by subtracting the ADRE at TOA by ADRE at the surface.

The cloud-screening (clear-sky) method in observations neglects the effects of aerosol above and below clouds. Absorption of reflected solar radiation by absorbing aerosol above clouds should result in larger radiative warming effect. The radiative cooling by scattering aerosol below clouds is not as strong as in the clear sky due to less sunlight penetrating the clouds. Both of the two factors will results in lower (more negative at TOA) radiative effect in clear-sky than that in all-sky. Therefore, the observation-derived ADRE in clear-sky provides an upper-limit of the model-estimated all-sky ADRE at TOA.

3 Results

3.1 Comparing MEIC and AR5 emission inventories

Figure 2 compares the MEIC and AR5 emission inventories in China. The spatial distributions of the two emission inventories are generally consistent. The MEIC emission rates in China are 14.59 Tg Sulfur (S)/year, 1.78 Tg Carbon (C)/year, 5.16 Tg C /year, 3.50 Tg C /year for SO_2 (including primary sulfate), BC, POM, and SOAG, respectively (Table S1) and are 10.11%, 11.59%, 11.44%, and 36.34% higher than the AR5 emissions, respectively. The emissions are mostly concentrated in eastern China where the MEIC emission rates are 13.60 Tg S/year, 1.59 Tg C/year, 4.38 Tg C/year, 2.86 C Tg/year for SO_2 (including primary sulfate), BC, POM, and SOAG, respectively, which are 12.57%, 13.35%, 12.04%, and 46.88% higher than the AR5 emissions, respectively. SO_2, BC and POM emissions in MEIC are generally higher in northern China and the Sichuan Basin than those in AR5, whereas they are lower in southern China. The SOAG are higher in MEIC than AR5 in most part of eastern China, especially in southern China. Both emission inventories highlight the emission "hotspots" in the Jing-Jin-Ji region, Henan, Shangdong, Jiangsu Provinces, and the Sichuan Basin. SO_2 industrial emission is the major contributor to the "hotspots". Industrial and domestic emissions result in the high POM and BC emission in these "hotspots". Dust emission is identical between the two runs since the same constrained surface wind speed drives the dust emission.

In addition to differences in the magnitudes and spatial patterns of the total emissions in 2009, there are large differences in the seasonality of two emission inventories (Fig. 3). The AR5 SO_2 and BC emissions do not have seasonal variations, and the POM emission features a weak variation due to biomass burning with a slightly lower emission in the winter. The MEIC emission is characterized by monthly variations for SO_2, BC, and POM that peak in the winter. SOAG shows a consistent seasonal variation that peaks in the summer in both the MEIC and the AR5 emissions because the emissions of biogenic VOCs (isoprene and monoterpenes) dominate the SOAG emission and peak in the summer.

3.2 Aerosol optical depth

Figure 4 shows the spatial distributions of the annual averaged AOD over China simulated by CAM5-MAM3 using the MEIC and the AR5 emissions in 2009. They are compared with the MODIS and MISR satellite AOD retrievals. The modeled AOD (including dust aerosol) averaged over eastern China using the MEIC emission is 0.25, which is 30.38% higher than the AOD with the AR5 emission (0.19) (Table 1). The impact of anthropogenic emissions on the modeled dust AOD is small (< 1.0% difference) due to slightly different removal rates of dust resulting from the internal mixing of dust with anthropogenic aerosols (e.g., sulfate). The modeled AOD with the MEIC emission is 45.10% lower than the MODIS AOD (0.46) and 37.16% lower than the MISR AOD (0.40). The modeled AOD with the AR5 emission is 57.95% lower than the MODIS AOD and 51.87% lower than the MISR AOD. The MEIC emission improves the AOD simulations by 12.85% relative to MODIS and 14.71% relative to MISR compared with the AR5 emission. This suggests that the emission

uncertainty (bias) could account for 22.18%-28.37% of the underestimation of AOD simulated by CAM5 with the AR5 emission in eastern China.

The dominant contributor to the total AOD is the sulfate aerosol followed by dust, POM, BC, and SOA in both emission runs (Table 1). The MEIC emission produces 17.40%-70.35% higher AODs of different anthropogenic aerosol species than the AR5 emission. The sensitivities of modeled AOD to the emission change between the two inventories are quite different for each aerosol species due to different aerosol refractive indexes. 12.04% of POM emission difference results in 70.35% of the AOD difference. In contrast, 46.88% of the SOAG emission difference leads to only 17.40% of the AOD difference of SOA.

Do the emission inventories produce the reasonable AOD spatial distribution in spite of the underestimated magnitudes? By comparing the spatial distribution of the emissions (Fig. 2) with the AOD distribution (Fig. 4), we found that the AOD distribution basically agree with the emission patterns of sulfate, dust, POM and dust aerosols, which contributes to about 85% of the total AOD. Fig. 4e and Fig. 4f shows the scaled MODIS and MISR AOD by one-half and two-thirds, respectively, which are approximately the ratios between the modeled AOD with the MEIC emission and observed AODs averaged over eastern China. It is found that the model generally reproduces the spatial distribution of MODIS and MISR retrieved AOD. The Jing-Jin-Ji Region, Sichuan Basin, Shandong, Henan, Aihui, Hunan, Hubei Provinces are characterized by higher AODs than other parts of China, which is consistent with the higher anthropogenic emissions in these regions.

Figure 5 shows the seasonal variation of longitudinal (100^{o}E to 124^{o}E) averaged AOD over eastern China. The CAM5 simulation using the MEIC emission captures the observed AOD maximums around 30^{o}N in the spring (February to May) and in the autumn (August to October) but the magnitudes are lower than the observations. The model results using the AR5 emission fail to capture the first maximum and underestimate the second one even more than the MEIC emission. By examining the model AOD components by species (Figure S1), the first maximum is mostly due to sulfate aerosol and to a less extend due to POM aerosol, and the second maximum is mostly due to sulfate. Sulfate AOD peaks in the summer because the production of sulfuric acid gas (H_2SO_4) is more efficient at higher temperatures. Wet scavenging due to the strong East Asian summer monsoon precipitation reduces the aerosol concentrations. This is evident in both the model results and the observations with minimal AODs in the summer between 20^{o}N to 30^{o}N. However, the modeled precipitation (mostly large-scale precipitation) extends further north in the summer compared with the Global Precipitation Climatology Project (GPCP) observations (not shown here). This causes the model to underestimate the AOD maximum around 30^{o}N in the summer in spite of evident sulfate production at this time and location.

The model simulates a maximum between 35^{o}N and 40^{o}N in early summer (from May to July), which is to the north of the observed AOD maximum.. This model maximum is mostly due to dust aerosol transported from the west, while the satellite retrievals do not show such strong dust emission and transport. Since the dust emissions are the same in the simulations using the MEIC and AR5 emissions, the difference of the modeled AOD maximums between 35^{o}N and 40^{o}N is mainly due to sulfate condensed on dust aerosol. We notice that the maximum AOD in the satellite retrieval occurs around 30^{o}N in early summer (May to July), as oppose to 35^{o}N to 40^{o}N as simulated by the model. The observed AOD maximum complies with the SO_2 emission maximum in early summer around 30^{o}N (Figure S2). Therefore, it is likely that this AOD maximum is due

to sulfate aerosol formation and it is heavily underestimated by the model. Since the uncertainty of SO_2 emission is relative low (±12%), this underestimation cannot be explained by emission alone. Other causes (e.g., missing nitrate, particle size distribution, aerosol hygroscopic growth, etc.) in the model are more responsible.

The satellite retrievals show another two AOD maximums around 22-25°N in March and September. The model simulates the first maximum by capturing the POM maximum at this time and location. We note that there is no strong POM emission and therefore the maximum possibly results from the reduced wet scavenging or low wind speeds. The model results do not show the second maximum or the peak is too weak. Figure 5 indicates that the MEIC emission improves the model performance in reproducing the AOD spatiotemporal distribution. However, there are still processes other than emission that need to be improved in order to reduce the discrepancy between model and observations. Among the possible processes, wet scavenging should be improved since it significantly affects the model results. The CAM5-MAM3 does not include the treatment of nitrate aerosol, which can be an important aerosol component in East Asia (Gao et al., 2014). The modeling of dust aerosol is of particular importance in northern China by contributing to the AOD maximum in autumn and providing the surface area for sulfate condensation.

Figure 6 shows the seasonal variation of monthly averaged AOD in 2009 at 12 AERONET sites in and around China. The model simulations using both emissions generally underestimate AOD compared with AERONET and MODIS observations. The model results in Beijing, Xianghe and Xinglong agree better with MISR observations in spring and winter. The modeled AODs in the MEIC emission run are higher and agree better with the observations than the AR5 emission run in Beijing, Xianghe, Taihu, and Hong Kong, where anthropogenic emissions are significant. In Beijing, Xianghe, and Xinglong the MODIS and MISR AODs are high in February, which are better simulated with the MEIC emission that has the seasonal variations of BC and POM emissions, whereas the AR5 run does not capture this feature because of a lack of seasonal variations of the emissions. In the summer, the observed seasonality in Beijing, Xianghe, and Xinglong features a maximum in July and a lower AOD in June, where the modeled AOD peaks in June. Model results show that dust aerosol dominates the modeled AOD maximum in June and both the dust and sulfate aerosol dominate in July at these sites. The dust aerosol maximum in June is also simulated at the upwind SACOL site. Dust aerosol is usually transported from SACOL to Beijing, Xianghe, and Xinglong. The satellite retrieved AOD shows a minor peak in June but smaller than that in April. This implies that the timing of the dust AOD maximums over northern China is not well simulated in the model. In addition, sulfate and other anthropogenic aerosols that contribute to the high AOD in the summer are underestimated in the model with both emission inventories. This comparison highlights the importance for better modeling the dust aerosol in northern China.

The Taihu site is in the southern China where the modeled AODs are underestimated at all seasons compared with observations. The model shows that the dominant aerosol species is sulfate in all the year, followed by POM in winter and SOA in the late summer. Sulfate aerosol peaks in September and June and SOA peaks in September. These peaks are observed in MODIS and MISR but are a factor of 2-3 larger than the modeled ones.

The impact of using the new emission inventory in China is also reflected in the modeled AODs in the downwind regions. AODs at the sites in 20-30°N (Taiwan and Hong Kong sites) are featured by the summer minimums in both observations and

model results due to the scavenging of aerosols by the summer monsoon precipitation. The model captures the seasonality but underestimates the AOD by a factor of 2-3. The MEIC emission has a significant impact on AOD in Hong_Kong_PolyU site in all seasons and only has a small impact in winter in Taiwan sites (NCU_Taiwan, EPA_Taiwan, and Chen-Kung_Univ). AODs at the sites north of 30^{o}N (Gwangju_GIST, Osaka, and Shirahama) are characterized by the AOD maximums in spring and June as observed by MODIS, MISR and AERONET. Model results indicate that sulfate aerosol is the main contributor to the AOD. The model captures the summer maximum at Gwangju_GIST site and the modeled AOD with the MEIC emission is higher than that with the AR5. The difference between the two emission inventories is not evident at Osaka and Shirahama.

Figure 7 shows the modeled SSA using the MEIC and AR5 emissions and the comparison to the observations by AERONET. The modeled SSA at Beijing, Xianghe, and Xinglong agree with the AERONET retrievals in the strong seasonal variation of lower SSA in the winter and higher SSA in the summer, indicating higher fractions of absorbing aerosols in the winter. However, the modeled SSAs are systematically lower than the AERONET retrievals. This indicates the significant underestimation of scattering aerosols (e.g., sulfate and POM), consistent with the AOD underestimation at these sites. The SSA simulated with the MEIC emission is lower than that using the AR5 emission by up to 0.05 in winter, which is consistent with the higher BC emission in the MEIC emission. The SSAs simulated with the MEIC emission in Taihu are slightly higher than that with the AR5 emission throughout the year, which is consistent with the higher MEIC sulfate emission. Outside Mainland China the modeled SSAs agree with AERONET retrievals reasonably well at the Hong Kong, Taiwan and Japanese sites, although underestimations can be still in some months.

3.3 Aerosol concentrations

Figure 8 compares the modeled surface concentrations of sulfate, BC, POM, and SOA with the chemical observations. The surface concentrations of these aerosol species are generally underestimated in the model, which is consistent with the AOD underestimation. The simulated surface concentrations of these species are improved by using the MEIC emission compared with those modeled by using the AR5 emission. The POM and BC surface concentrations are significantly improved by the MEIC emission due to higher emission rates especially in the winter. The sulfate aerosol concentration is underestimated by about a factor of 3 (the linear regression slope of 0.35) using the MEIC emission but is improved compared with about a factor of 5 (the linear regression slope of 0.18) using the AR5 emission. The root mean square errors (RMSEs) using the MEIC emission are 10.01, 14.63, 3.32, 6.58 μg m^{-3} for sulfate, POM, BC, and SOA, respectively, which are smaller than RMSEs of 13.38, 19.21, 3.97, 8.38 μg m^{-3} if using the AR5 emission. The correlation coefficients (R^2) between model simulations and observations of all these species are also improved. Considering that most observations are carried out at single points and at altitudes close to the surface, the underestimation could be partly due to the coarse model horizontal and vertical resolutions. The model with a coarse horizontal resolution does not account for the subgrid variability of aerosols (Qian et al., 2010). With the coarse vertical resolution, the aerosol species are assumed to be well mixed in the bottom model layer with a thickness of about 120 m.

Figure 9 shows the seasonal variations of surface concentrations of sulfate, POM, and BC simulated with the MEIC and AR5 emissions and the comparisons with the chemical composition observations of $PM_{2.5}$ at 10 locations in China. Note that CAM5-MAM3 simulates the aerosols of diameter less than 3.65 μm so the values shown here represent the upper limit of the simulated concentrations. The MEIC emission improves the modeled aerosol concentrations compared with the AR5 emission for all the three aerosol species. The seasonal variations of surface concentrations of POM and BC are mainly determined by their emissions. As shown in Fig. 3, there are no seasonal variations of POM and BC in the AR5 emissions. By introducing the seasonally varied MEIC emissions of POM and BC, the seasonal changes of POM and BC surface concentrations are better simulated with higher concentrations in the winter and lower concentrations in the summer, which are consistent with the observations. The impact of emission on the seasonal cycle of sulfate surface concentrations is less obvious since sulfate aerosol production depends on meteorology (i.e., temperature and precipitation). The sulfate concentrations in northern China (Harbin, Chengde, Shangdianzi, Beijing, Tianjin, Shijiazhuang, Zhengzhou) are characterized by the summer maximums in both model results and observations. The sulfate concentrations in the southern cities (Xiamen and Guangzhou) do not have the summer maximum due to the Asian summer monsoon with strong winds and precipitation.

The emission of SO_2 peaks in the winter in northern China (Harbin, Chengde, Shangdianzi, Beijing, Tianjin, Shijiazhuang, and Zhengzhou) due to heating in the domestic section. However, the modelled sulfate aerosol concentrations show their minimum in the winter (Figure 9), which is commonly seen for many climate models (personal communication with Prof. Hong Liao from Nanjing University of Information Science & Technology). Obviously, the surface concentrations cannot be explained by emissions alone, and atmospheric physical and chemical processes are more responsible for the low bias. We examine the processes that determine the sulfate aerosol concentrations in the model, including gas-phase and aqueous-phase production, the dry removal and wet scavenging, as well as the controlling meteorological variables (Figure S3). The simulated seasonal variations of surface concentrations of sulfate aerosol are controlled by the gas-phase and aqueous-phase production processes, as oppose to the emission of SO_2. The gas-phase chemistry is most active in the summer due to the temperature-dependence of the reaction rate in the photochemical oxidation of SO_2 by OH. The aqueous-phase formation of sulfate aerosol also peaks in the summer due to high relative humidity. Although the MEIC SO_2 emissions peak in the winter, both gas-phase and aqueous-phase oxidations are inefficient in the winter, which results in lower concentrations of sulfate aerosol than in the summer.

The seasonal variations of modeled sulfate aerosol concentrations are verified by some observations (Zhao et al., 2013; Zhang et al., 2013; Geng et al., 2015). However, observations from CAWNET (Zhang et al., 2012) show that sulfate aerosol concentrations in the northern Chinese cities (Gucheng and Zhengzhou in Figure S4) peak in the winter as opposed to summer in spite of a minor maximum in the summer, which is consistent with our general recognition. The contrasting result in observations could be due to different location and time. The difference between the simulated and the observed seasonal variations by the CAWNET may reveal that some mechanisms of sulfate aerosol formation in the winter over China are missing in the model. The importance of sulfate production through heterogeneous reactions of SO_2 on deliquescence

preexisting particles catalyzed by transition mental ions, which can increase PM2.5 concentrations and the mass fractions of secondary inorganic aerosols in the wintertime hazes of northern China (Wang et al. 2014; Huang et al., 2014; Zheng et al, 2015; Chen et al., 2016; Dong et al., 2016). The coexistence of NO_2 and SO_2 also promotes sulfate production (He et al., 2014; Wang et al., 2014). The aqueous-phase oxidation of SO_2 by NO_2 (Wang et al., 2016) or O_3 (Palout et al., 2016) is efficient to form sulfate aerosol under high relative humidity and NH_3 neutralization conditions. One thing to notice is that aqueous-phase oxidation occurs only in cloud droplets in the model. The aqueous-phase oxidation of SO_2 by NO_2 on pre-existing aerosols is not modeled by CAM5-MAM3, which is important in China (Wang et al., 2016).

Having the same "constrained" meteorology for the two runs with different emission inventories provides us with an opportunity to examine the impact of emission on the seasonality of aerosols versus the impact of meteorology. The longitudinal averaged BC burden in the MEIC emission run shows a strong seasonal variation with higher burden between 25 and 40 ^{o}N in the winter (Fig. 10a), which is correspondent with the seasonal variation of BC emission (Fig. 10b). We note that there is no seasonal variation for BC aerosol in the AR5 emission (Fig. 10d), and thus the seasonal variation of BC concentration can only be due to the impact of meteorology in the AR5 emission run (Fig. 10c). Fig. 10 indicates that seasonal variations of both the emission and meteorology play important roles in determining the seasonal variation of BC concentrations.

The impacts of emission on seasonal variations of primary (e.g., BC) and secondary aerosols (e.g., sulfate) are different. Figure 11 shows that the seasonal variation of the differences in the longitudinally averaged BC burden between the two emission runs resembles closely the pattern of difference in the BC emission. However, the dependence of seasonal variation of sulfate burden on the SO_2 emission is less evident (Fig. 11c and Fig. 11d). The large difference of sulfate burden between the two emission runs is obviously aligned with high temperatures between 30 and 40 ^{o}N in the summer (May to July) (Fig. 11e) where evident SO_2 emission difference exists there in the summer. It is because H_2SO_4 gas production to form sulfate aerosol are favored at higher temperatures. In contrast, although there is a significant difference in the SO_2 emission between 34 and 40 ^{o}N in the winter (November to March) the sulfate burden difference is not as evident due to the fact that low temperatures inhibit the sulfate production. Wet scavenging by clouds and precipitation helps to reduce the concentrations and the absolute concentration differences in southern China during the spring and summer (Fig. 11f and Fig. 11g). Stagnant wind field that propagates from 22^{o}N to 30^{o}N in the winter to 30^{o}N to 40^{o}N in the spring (Fig. 11h) also contributes to the large differences of BC and sulfate burdens between the MEIC emission and AR5 emission in corresponding seasons and regions. Diffusion of sulfate aerosol due to higher wind speeds north of 35 ^{o}N in the winter also helps to explain the smaller sulfate burden difference in spite of the evident SO_2 emission difference there. Thus, compared to primary aerosols, the spatiotemporal patterns of secondary aerosol burdens follow less closely to their emissions.

3.4 Aerosol direct radiative effect

Figure 12 shows the spatial distribution of annual averaged shortwave aerosol DREs in China simulated using the MEIC and the AR5 emissions due to all aerosol species (sulfate, POM, BC, SOA, dust and sea salt) at TOA, surface, and in the

atmosphere. The TOA radiative cooling effect is evident in eastern China due to anthropogenic aerosols. At some parts of the southwestern China the ADRE at TOA is positive due to strong BC absorption in the atmosphere. The most pronounced surface cooling and atmospheric warming are located in the northern China and the Sichuan Basin, which is consistent with the spatial patterns of the emissions. In these locations the surface and atmospheric differences of the ADREs between the MEIC and the AR5 emissions are also significant.

As shown in Table 2 the annual averaged cooling effect at TOA is reduced (more negative) by -0.19 W m^{-2} (63.32%) by all aerosols using the MEIC emission (-0.50 W m^{-2}) than the AR5 emission (-0.31 W m^{-2}). The small TOA ADRE is the sum of the large surface cooling and atmospheric warming effects. At the surface there is a strong cooling effect of -12.76 W m^{-2} using the MEIC emission, which is reduced (more negative) by -2.42 Wm^{-2} (23.42%) compared with that using the AR5 emission (-10.34 W m^{-2}). The atmospheric warming effect of all aerosols using the MEIC emission is estimated to be 12.26 W m^{-2}, which is 2.23 W m^{-2} (22.20%) stronger than the estimation made by the AR5 emission (10.03 W m^{-2}) over eastern China.

Table 2 also shows the annually averaged ADREs over eastern China by individual aerosol species (sulfate, BC, and POM). The ADREs of SOA are not shown due to its large emission uncertainty. Due to larger AODs simulated with the MEIC emission, the ADREs by every individual aerosols are larger than the ADREs using the AR5 emission by 29.91% to 66.03% at TOA. The ADRE percentage differences are similar to the AOD percentage differences as listed in Table 1. Tables 1 and 2 show that 12.04% to 46.88% difference of the anthropogenic emission rates of various aerosol species results in 30.38% difference of the total AOD of all species (including anthropogenic and natural aerosols), about 22% difference of the surface and atmosphere ADREs, and about 63% of the ADRE at TOA of all aerosol species over eastern China. The impacts of the emission on AOD and ADRE are significant.

The normalized radiative effect (NRE) represents the radiative effect efficiency per unit aerosol optical depth (Schultz et al., 2006). The light scattering aerosols (sulfate and POM) have very similar negative NREs (-14.34 and -14.71 W m^{-2} τ_{aer}^{-1} with the MEIC emission hereafter). The light absorbing BC aerosol shows a much higher positive NRE (122.40 W m^{-2} τ_{aer}^{-1}) which is comparable to the mean NREs of the AeroCom models (153 W m^{-2} τ_{aer}^{-1}) considering the wide range of the estimates among the models (28 to 270 W m^{-2} τ_{aer}^{-1}) (Schulz et al., 2006). This indicates that the ADREs are much more sensitive to BC aerosol burden than the other aerosol species. This highlights the importance of the BC emission and concentration to correctly represent the ADRE in the model. BC also makes the largest contributor to the ADRE in the atmosphere and at the surface. The NREs of BC are much higher than the other aerosols species, especially the warming in the atmosphere (281.22 Wm^{-2} τ_{aer}^{-1}). We note that the ADREs of light scattering aerosols (sulfate and POM) in the atmosphere are also warming effects. The explanation is that coating of these scattering aerosols on BC increases the absorption capability of the internally mixed aerosol particles (i.e., particles in the same aerosol mode with BC) (Chung et al., 2011).

The impact of emission on the spatial distributions of ADRE of BC is more significant compared with the meteorological effects. Since there is no seasonal variation of BC emission in the AR5 dataset, the resultant different spatial distributions of

BC aerosol and the ADRE between summer and winter are due to the monsoon circulation and precipitation (Jiang et al., 2015). The averaged ADREs over eastern China in the winter (-3.37 W m^{-2} at surface and 5.40 W m^{-2} in the atmosphere) are close to the ADREs in the summer (-3.49 W m^{-2} at surface and 5.75 W m^{-2} in the atmosphere) using the AR5 emission. Due to higher MEIC BC emission in the winter, the cooling effect of BC at the surface is much more significant using the MEIC emission (-5.86 W m^{-2}) than the AR5 emission averaged over eastern China (Fig. 13). Likewise the warming effect of BC in the atmosphere is 9.31 W m^{-2}, which is nearly twice as much as that using the AR5 emission (Fig. 14). Driven by the same constrained meteorology, the MEIC emission results in stronger seasonal variation of ADRE of BC than the AR5 emission.

Figure 15 shows the comparison between the measured and modeled ADREs at TOA, surface, and in the atmosphere in China. Observations from 25 nationwide stations shows that clear-sky ADREs are characterized by a strong radiative heating in the atmosphere, which implies a substantial warming in the atmosphere and cooling at the surface (Li et al., 2007; Li et al., 2010). This implies the enhanced haze pollution in winter due to the strong atmospheric inversion (Wang et al., 2015; Ding et al., 2016). Model simulations show small ADREs (-4 to 1 W m^{-2}) at TOA with both the MEIC and AR5 emission inventories, while the measurements gives a much larger range of ADREs at TOA (-14 to 2 W m^{-2}). At the surface and in the atmosphere, the modeled ADREs using the MEIC emission inventory at most locations are within a factor of 2 compared with observations. The MEIC emission inventory produces better agreement with the observations than the AR5 emission inventory. Overall, the model underestimates the ADREs at the surface and in the atmosphere compared with observations due to underestimated aerosol loading, which results in a smaller range of the ADREs at TOA than the observations.

4. Decadal trend of ADRE

Figure 16 shows the MEIC's SO_2, BC, and OC emission trends from 2002 to 2012 in eastern China. Since spatially-gridded MEIC emission data are only available for 2008, 2010, and 2012, we scale the spatial distribution and seasonal variation of other years during the period to the 2008 gridded emission with the annual emissions. The annual emission rates of each species (SO_2, BC, OC) are estimated by the MEIC developer team. Each species in different sectors (power, energy, residential, and transportation) has a different scaling factor. The annual trends are consistent with other researches (Lu et al., 2011; Lei et al., 2009) although the absolute values are different. We use the MEIC estimations because their fuel usage is based on China Energy Statistical Yearbook (CESY) as this dataset is based on the same algorithm as the gridded MEIC emission data that we used for 2009.

Figure 17 shows that the change of the ADREs from 2002 to 2012 relative to those in 2002 are 0.01~0.16 W/m^2, -0.44~0.39 W/m^2, and -0.23~0.51 W/m^2 at TOA, surface and in the atmosphere, respectively. The decadal trend of ADRE agrees with the trend of emissions as shown in Figure 16. The warming in the atmosphere and the cooling at the surface enhanced with the increase of emissions of SO_2, BC, and POM from 2003 to 2006. The ADRE at TOA increased slightly indicating more energy retained in the atmosphere-earth system. From 2006 to 2009, the changes of ADREs were not significant due to the stabilized emission of BC. Since 2010, the warming in the atmosphere and the cooling at the surface increased due to the increased emission of SO_2 and BC. The changes of ADREs at surface and in the atmosphere from 2002 to 2003 may reflect

the complicated interactions between sulfate and BC/OC in eastern China, enhancing the BC/OC wet scavenging due to sulfate coating.

Comparing with the difference between the ADREs simulated by MEIC and AR5 emission inventories in 2009, which is -0.19 W/m^2, -2.42 W/m^2, 2.23 W/m^2 at TOA, surface and in the atmosphere, respectively, the decadal change of ADRE at TOA is comparable to the uncertainty range introduced by the emission inventories. The decadal changes of ADRE at surface and in the atmosphere are smaller than the uncertainties by using the two different emissions. The change of ADRE at TOA in eastern China due to the change of emission structure is not significantly different than the difference estimation of emissions, although the magnitude of changes at surface and in the atmosphere is smaller. It highlights the uncertainty of the emission inventories and the need of constraining the emission inventories of aerosol and precursors by in-situ and satellite observations.

5 Summary and Conclusions

Anthropogenic aerosols in East Asia may have substantial effects on regional air quality and climate. However, CMIP5 models generally have low biases in anthropogenic aerosol burdens in this region (Shindell et al., 2013), and thus the aerosol effects may be underestimated. The reasons behind the low biases are unclear, but may include the bias in aerosol emissions, missing of some aerosol processes, coarse model resolutions, etc. In this study, we simulated the aerosol concentrations, optical depth, and the radiative effects in eastern China using the Community Atmospheric Model version 5 with the 3-mode model aerosol module (CAM5-MAM3). The "constrained" meteorology is applied to avoid the ambiguity from model predicted meteorological bias. A technology-based emission inventory, Multi-scale Emission Inventory for China (MEIC), was implemented into CAM5-MAM3 and results were compared with the default IPCC AR5 emission inventory.

We found that the MEIC emission improves the annual mean AOD simulations in eastern China by 12.85% compared with the MODIS observations and 14.71% compared with the MISR observations, which explains 22.18%-28.37% of the AOD underestimation simulated with the AR5 emission. The MEIC emission generally reproduces the AOD spatial distribution although AOD is still underestimated compared with the MODIS and MISR satellite retrievals. The MEIC emission run captures the AOD maximums around 30^{o}N in the spring and the autumn better than the AR5 emission run. However, both emission runs underestimate the AOD maximum around 30^{o}N in the summer, which coincides with the modeled summer monsoon precipitation. Wet scavenging by summer monsoon precipitation should be reasonably represented since it significantly affects the model AODs. The modeling of dust aerosols is also of particular importance in northern China.

The simulated surface concentrations of anthropogenic aerosol species are improved by using the MEIC emission compared with that modeled by the AR5 emission. Seasonal variation of the MEIC emission leads to better agreement with the observed surface concentrations of primary aerosols (i.e., POM and BC) than the AR5 emission, while the seasonal variations of secondary aerosol species (i.e., sulfate) depend less on the emission. The difference of the primary aerosol burdens in the two emission runs agree with the difference of the emission patterns, while the secondary aerosol concentrations depend on both the emission and the meteorological factors (e.g., temperature, precipitation, wind). The

emission of SO_2 in the northern cities peaks in the winter due to domestic heating. Since both the gas-phase and in-cloud aqueous-phase formation of sulphate aerosol are simulated to peak in the summer, the surface concentrations of sulphate aerosol peak in the summer. The seasonal variation is different from observations by some observations (e.g., CAWNET), which cannot be explained by the emission alone. This may reveal that some mechanisms, such as production through heterogeneous reactions of SO_2 on aerosols, which is not currently included in the model, can be important sources of sulfate aerosol in the winter.

Different emissions also have substantial effects on the aerosol radiative effects. By using the MEIC emission, the annual averaged ADREs at TOA and at the surface over eastern China are reduced (more negative) by -0.19 W m^{-2} and -2.42 W m^{-2}, respectively, while the warming in the atmosphere is increased by 2.23 W m^{-2}. The ADREs between the MEIC and AR5 emissions with all aerosols species (including natural dust) increases by 63.32%, 23.42%, and 22.20% at TOA, surface and in the atmosphere, respectively. The ADRE is much more sensitive to BC aerosol burden than the other aerosol species. Due to the higher MEIC BC emission in the winter, the warming effect of BC in the atmosphere and the cooling effect at the surface are much higher than those using the AR5 emission. Over eastern China about 12% to 47% difference of the emission rates of different aerosol species results in 30.38% difference of the total AOD, about 22% difference of the surface and atmosphere ADREs, and about 63% of the TOA ADRE. The impacts of the emission on AOD and ADRE are significant.

By examine the change of ADRE from 2002 to 2012 using the estimation of emissions made by the MEIC developer team, we find that the change of ADRE at TOA in eastern China due to the change of emission structure is not significantly different than that estimated by the MEIC and AR5 emissions in 2009. However, the decadal changes of ADRE at surface and in the atmosphere are smaller than the uncertainties by using the two different emissions. This indicates that there is an urgent need to constrain the emission inventories of aerosol and precursors by in-situ and satellite observations.

This research highlights the critical importance of improving aerosol and precursor emissions for the modeling of aerosols and aerosol radiative effects in East Asia. We note that modeled aerosol AOD is still underestimated in CAM5 even with the MEIC emission. The CAM5 model with a horizontal resolution of $0.9^{o}\times1.25^{o}$ may miss the subgrid aerosol variability (Qian et al., 2010) as well as not able to capture the collocation between aerosols and clouds important for aerosol wet scavenging (Ma et al., 2014). CAM5-MAM3 may also miss some important aerosol species (e.g., nitrate) which can have similar mass burdens as sulfate in eastern China (Gao et al., 2014). Current work is under the way to improve the model resolution and to implement nitrate aerosol in CAM5-MAM3. The impacts of these new developments on aerosols in East Asia will then be evaluated.

Acknowledgements. The authors would like to acknowledge the use of computational resources (ark:/85065/d7wd3xhc) at the NCAR-Wyoming Supercomputing Center provided by the National Science Foundation and the State of Wyoming, and supported by NCAR's Computational and Information Systems Laboratory. This work was supported by the Ministry of Science and Technology of China through grant 2013CB955804. Both T. Fan and C. Zhao were supported by the

Fundamental Research Funds for the Central Universities (Grant No. 310400090). We thank the AERONET PI investigators and their staff for establishing and maintaining the 12 sites used in this investigation.

References

Bond, T. C. and Bergstrom, R. W.: Light Absorption by Carbonaceous Particles: An Investigative Review, Aerosol Sci. Tech., 40, 27–67, 2006.

Chang, W., Liao, H., Xin J., Li, Z., Li, D., Zhang, X.: Uncertainties in anthropogenic aerosol concentrations and direct radiative forcing induced by emission inventories in eastern China, Atmos. Res., 166, 129-140, 2015.

Chen, D., Liu, Z., Fast, J., and Ban, J.: Simulations of sulfate-nitrate-ammonium (SNA) aerosols during the extreme haze events over northern China in October 2014. Atmos. Chem. Phys., 16, 10707-10724, doi:10.5194/acp-16-10707-2016, 2016.

Chen, D., Wang, Y., McElroy, M. B., He, K., Yantosca, R. M., and Sager, P. Le: Regional CO pollution and export in China simulated by the high-resolution nested-grid GEOS-Chem model, Atmos. Chem. Phys., 9(11), 3825-3839, 2009.

Chung, C. E., Lee, K., and Müller, D.: Effect of internal mixture on black carbon radiative forcing, Tellus B, 64, 2011.

Dee, D. P., Uppala S. M., Simmons A. J., Berrisford, P., Poli, P., Kobayashi, S., Andrae, U., Balmaseda, G., Balsamo, M. A., Bauer, P., Bechtold, P., Beljaars, A. C. M., van de Berg, L., Bidlot, J., Bormann, N., Delsol, C., Dragani, R., Fuentes, M., Geer, A. J., Haimberger, L., Healy, S. B., Hersbach, H., Hólm, E. V., Isaksen, L., Kållberg, P., Köhler, M., Matricardi, M., McNally, A. P., Monge-Sanz, B. M., Morcrette, J.-J., Park, B.-K., Peubey, C., de Rosnay, P., Tavolato, C., Thépaut, J.-N. and Vitart F.: The ERA Interim reanalysis: Configuration and performance of the data assimilation system, Q. J. Roy., Meteor. Soc., 137, 553-597, 2011.

Dentener, F., Kinne, S., Bond, T., Boucher, O., Cofala, J., Generoso, S., Ginoux, P., Gong, S., Hoelzemann, J. J., Ito, A., Marelli, L., Penner, J. E., Putaud, J.-P., Textor, C., Schulz, M., van der Werf, G. R., and Wilson, J.: Emissions of primary aerosol and precursor gases in the years 2000 and 1750 prescribed data-sets for AeroCom, Atmos. Chem. Phys., 6(12), 4321-4344, 2006.

Ding, A. J., Huang, X., Nie, W., Sun, J. N., Kerminen, V.-M., Petäjä, T., Su, H., Cheng, Y. F., Yang, X.-Q., Wang, M. H., Chi, X. G., Wang, J. P., Virkkula, A., Guo, W. D., Yuan, J., Wang, S. Y., Zhang, R. J., Wu, Y. F., Song, Y., Zhu, T., Zilitinkevich, S., Kulmala, M., and Fu, C. B.: Enhanced haze pollution by black carbon in megacities in China, Geophys. Res. Lett., 43, 2873-2879,doi:10.1002/2016GL067745, 2016.

Dong, X., Fu, J. S., Huang, K., Tong, D., and Zhuang, G.: Model development of dust emission and heterogeneous chemistry within the Community Multiscale Air Quality modeling system and its application over East Asia. Atmos. Chem. Phys., 16, 8157-8180, doi:10.5194/acp-16-8157-2016, 2016.

Emmons, L. K., Walters S., Hess, P. G., Lamarque, J.-F., Pfister, G. G., Fillmore, D., Granier, C., Guenther, A., Kinnison, D., Laepple, T., Orlando, J., Tie, X., Tyndall, G., Wiedinmyer, C., Baughcum, S. L., and Kloster, S.: Description and

evaluation of the Model for Ozone and Related chemical Tracers, version 4 (MOZART-4), Geosci. Model Dev., 3(1): 43-67, 2010.

Fu, T.-M., Cao. J. J., Zhang, X. Y., Lee, S. C., Zhang, Q., Han, Y. M., Qu, W. J., Han, Z., Zhang, R., Wang, Y. X., Chen, D., and Henze, D. K.: Carbonaceous aerosols in China: top-down constraints on primary sources and estimation of secondary contribution, Atmos. Chem. Phys., 12(5): 2725-2746, 2012.

Gao, Y., Zhao, C., Liu, X., Zhang, M., and Leung, L.-R.: WRF-Chem simulations of aerosols and anthropogenic aerosol radiative forcing in East Asia, Atmos. Environ., 92, 250–266, doi:10.1016/j.atmosenv.2014.04.038, 2014.

Geng, N., Wang, J., Xu, Y., Zhang, W., Chen, C., and Zhang, R.: PM2.5 in an industrial district of Zhengzhou, China: chemical composition and source apportionment, Particuology, 11(1), 99-109, 2013.

Ghan, S. J.: Technical Note: Estimating aerosol effects on cloud radiative forcing, Atmos. Chem. Phys., 13, 9971–9974, doi:10.5194/acp-13-9971-2013, 2013.

Giorgi, F., Jones, C., and Asrar, G. R.: Addressing climate information needs at the regional level: the CORDEX framework, WMO Bulletin, 58(3), 175–183, 2009.

Guenther, A., Karl, T., Harley, P., Wiedinmyer, C., Palmer, P. I., and Geron, C.: Estimates of global terrestrial isoprene emissions using MEGAN (Model of Emissions of Gases and Aerosols from Nature), Atmos. Chem. Phys., 6, 3181–3210, 2006.

He, H., Wang, Y., Ma, Q., Ma, J., Chu, B., Ji, D., Tang, G., Liu, C. Zhang, H., and Hao, J.: Mineral dust and NOx promote the conversion of SO2 to sulfate in heavy pollution days. Sci. Rep., 4, 4172, doi:10.1038/srep04172, 2014.

He, J., and Zhang, Y.: Improvement and further development in CESM/CAM5: gas-phase chemistry and inorganic aerosol treatments, Atmos. Chem. Phys., 14, 9171-9200, 2014.

Hess, M., Koepke, P., and Schult, I.: Optical properties of aerosols and clouds: The software package OPAC, B. AM. Meteorol. Soc., 79(5), 831-844, 1998.

Hsu, N. C., Tsay, S. C., King, M. D., and Herman, J. R.: Aerosol properties over bright-reflecting source regions, IEEE T. Geosci. Remote, 42(3), 557-569, 2004.

Huang, X., Song, Y., Zhao, C., Li, M., Zhu, T., Zhang, Q., and Zhang, X.: Pathways of sulfate enhancement by natural and anthropogenic mineral aerosols in China. J. Geophys. Res., 119, 14165-14179, doi:10.1002/2014JD022301, 2014.

Iacono, M. J., Delamere, J. S., Mlawer, E. J., Shephard, M. W., Clough, S. A., and Collins, W. D.: Radiative forcing by long-lived greenhouse gases: Calculations with the AER radiative transfer models, J. Geophys. Res.-Atmos, 113(D13), D13103, doi:10.1029/2008jd009944, 2008.

Jiang, Y., Yang, X. Q., Liu, X.: Seasonality in anthropogenic aerosol effects on East Asian climate simulated with CAM5, J. Geophys. Res.-Atmos, 120(20), doi:10.1002/2015JD023451, 2015.

Jones, C., Giorgi, F., and Asrar. G.: The coordinated regional downscaling experiment: CORDEX An international downscaling link to CMIP.CLIVAR Exchanges, 16(2), 34–40, 2011.

Klimont, Z., Cofala, J., Xing, J., Wei, W., Zhang, C., Wang, S., Kejun, J., Bhandari, P., Mathura, R., Purohit, P., Rafaj, P., Chambers, A., Amann, and M., Hao, J.: Projections of SO2, NOx, and carbonaceous aerosols emissions in Asia, Tellus B, 61, 602-617, doi:10.1111/j.1600-0889.2009.00428.x, 2009.

Lamarque, J. F., Bond, T. C., Eyring, V., Granier, C., Heil, A., Klimont, Z., Lee, D., Liousse, C., Mieville, A., Owen, B., Schultz, M. G., Shindell, D., Smith, S. J., Stehfest, E., Van Aardenne, J., Cooper, O. R., Kainuma, M., Mahowald, N., McConnell, J. R., Naik, V., Riahi, K., and van Vuuren, D. P.: Historical (1850–2000) gridded anthropogenic and biomass burning emissions of reactive gases and aerosols: methodology and application, Atmos. Chem. Phys., 10(15), 7017-7039, 2010.

Lei, Y., Zhang, Q., He, K., and Streets, D.G.: Primary anthropogenic aerosol emission trends for China, 1990–2005, Atmos. Chem. Phys., 11(3): 931-954, 2011.

Levy, R. C., Remer, L. A., Kleidman, R.G., Mattoo, S., Ichoku, C., Kahn, R., and Eck, T.F.: Global evaluation of the Collection 5 MODIS dark-target aerosol products over land, Atmos. Chem. Phys., 10(21),10399-10420, 2010.

Li, B., Gasser, T., Ciais, P., Piao, S., Tao, S., Balkanski, Y., Hauglustaine, D., Boisier, J.-P., Chen, Z., Huang, M., Li, L.Z., Li, Y., Liu, H., Liu, J., Peng, S., Shen, Z., Sun, Z., Wang, R., Wang, T., Yin, G., Yin, Y., Zeng, H., Zeng, Z., and Zhou, F.: The contribution of China's emissions to global climate forcing, Nature, 531(7594): 357-361, 2016.

Li, C., Zhang, Q., Krotkov, N. A., Streets, D. G., He, K., Tsay, S.-C., and Gleason, J. F.: Recent large reduction in sulfur dioxide emissions from Chinese power plants observed by the Ozone Monitoring Instrument, Geophys. Res. Lett., 37, L08807, doi:10.1029/2010GL042594, 2010.

Li, M., Zhang, Q., Streets, D. G., He, K. B., Cheng, Y. F., Emmons, L. K., Huo, H., Kang, S. C., Lu, Z., Shao, M., Su, H., Yu, X., and Zhang, Y.: Mapping Asian anthropogenic emissions of non-methane volatile organic compounds to multiple chemical mechanisms, Atmos. Chem. Phys., 14, 5617–5638, doi:10.5194/acp-14-5617-2014, 2014.

Li, Z., Xia, X., Cribb, M, Mi,W., Holben,B., Wang, P., Chen, H., Tsay S. C., Eck, T. F., Zhao, F., Dutton, E. G., and Dickerson, R. E.: Aerosol optical properties and their radiative effects in northern China, J. Geophys. Res., 112, D22S01, doi:10.1029/2006JD007382, 2007.

Li, Z., Lee, K. H., Wang, Y., Xin, J., Hao, W.-M.: First observation based estimates of cloud free aerosol radiative forcing across China, J. Geophys. Res.-Atmos., 115(D7), 2010.

Li, Z., Lau, W.K., Ramanathan, V., Wu, G., Ding, Y., Manoj, M.G., Liu, J., Qian, Y., Li, J., Zhou, T., Fan, J., Rosenfeld, D., Ming, Y., Wang, Y., Huang, J., Wang, B., Xu, X., Lee, S.-S., Cribb, M., Zhang, F., Yang, X., Takemura, T., Wang, K., Xia, X., Yin, Y., Zhang, H., Guo, J., Zhai, P.M., Sugimoto, N., Babu, S.S., Brasseur, G.P.: Aerosol and Monsoon Climate Interactions over Asia, Geophys. Rev., in review.

Liao, H., Chang, W., Yang, Y.: Climatic effects of air pollutants over china: A review, Adv. Atmos. Sci., 32(1): 115-139, 2015.

Liu, F., Beirle, S., Zhang, Q., Dörner, S., He, K. B., and Wagner T.: NOx lifetimes and emissions of hotspots in polluted background estimated by satellite observations, Atmos. Chem. Phys., 16, 5283-5298, doi:10.5194/acp-16-5283-2016, 2016.

Liu, X., Zhang, Y., Xing J., Zhang, Q., Wang, K., Streets, D.G., Jang, C., Wang, W., and Hao, J.: Understanding of regional air pollution over China using CMAQ, part II. Process analysis and sensitivity of ozone and particulate matter to precursor emissions, Atmos. Environ., 44, 3719-3727, doi:10.1016/j.atmosenv.2010.03.036, 2010.

Liu X., Easter, R. C., Ghan, S. J., Zaveri, R., Rasch, P., Shi, X., Lamarque, J.-F., Gettelman, A., Morrison, H., Vitt, F., Conley, A., Park, S., Neale, R., Hannay, C., Ekman, A. M. L., Hess, P., Mahowald, N., Collins, W., Iacono, M. J., Bretherton, C. S., Flanner, M. G., and Mitchell, D.: Toward a minimal representation of aerosols in climate models: description and evaluation in the Community Atmosphere Model CAM5, Geosci. Model Dev., 5, 709–739, doi:10.5194/gmd-5-709-2012, 2012.

Liu, Y., Huang, J., Shi, G., Takamura, T., Khatri, P., Bi, J., Shi, J., Wang, T., Wang, X., and Zhang, B.: Aerosol optical properties and radiative effect determined from skyradiometer over Loess Plateau of Northwest China, Atmos. Chem. Phys., 11, 11455-11463, 2011.

Lu, Z., Zhang, Q., and Streets, D. G.: Sulfur dioxide and primary carbonaceous aerosol emissions in China and India, 1996–2010, Atmos. Chem. Phys., 11, 9839–9864, doi:10.5194/acp-11-9839-2011, 2011.

Ma, P.-L., Rasch, P. J., Wang, H., Zhang, K., Easter, R. C., Tilmes, S., Fast, J. D., Liu, X., Yoon, J.-H., and Lamarque, J.-F. The role of circulation features on black carbon transport into the Arctic in the Community Atmosphere Model version 5 (CAM5), J. Geophys. Res. Atmos., 118, doi:10.1002/jgrd.50411, 2013.

Ma, P.-L., Rasch, P. J., Fast, J. D., Easter, R. C., Gustafson Jr.,W. I., Liu, X., Ghan, S. J., and Singh, B.: Assessing the CAM5 physics suite in the WRF-Chem model: implementation, resolution sensitivity, and a first evaluation for a regional case study, Geosci. Model Dev., 7, 755–778, doi:10.5194/gmd-7-755-2014, 2014.

Ohara, T., Akimoto, H., Kurokawa, J., Horii, N., Yamaji, K., Yan, X., and Hayasaka, T.: An Asian emission inventory of anthropogenic emission sources for the period 1980-2020, Atmos. Chem. Phys., 7, 4419–4444, doi:10.5194/acp-7-4419-2007, 2007.

Paulot F, Fan S, Horowitz L W.: Contrasting seasonal responses of sulfate aerosols to declining SO2 emissions in the Eastern US: implications for the efficacy of SO2 emission controls, Geophys. Res, Lett., 2016.

Qian, Y., Gustafson Jr., W.I., Fast, J.D.: An investigation of the sub-grid variability of trace gases and aerosols for global climate modelling, Atmos. Chem. Phys.,10, 6917-6946, 2010.

Schulz, M., Textor, C., Kinne, S., Balkanski, Y., Bauer, S., Berntsen, T., Berglen, T., Boucher, O., Dentener, F., S. Guibert, Isaksen, I. S. A., Iversen, T., Koch, D., Kirkevåg, A., Liu, X., Montanaro, V., Myhre, G., Penner, J. E., Pitari, G., Reddy, S., Seland, Ø., Stier, P., and Takemura, T.: Radiative forcing by aerosols as derived from the AeroCom present-day and pre-industrial simulations, Atmos. Chem. Phys., 6(12), 5225-5246, 2006.

Seinfeld, J. H. and Pandis, S. N.: Atmospheric chemistry and physics: from air pollution to climate change, John Wiley & Sons, 1998.

Shindell, D. T., Lamarque, J.-F., Schulz, M., Flanner, M., Jiao, C., Chin, M., Young, P. J., Lee, Y. H., Rotstayn, L., Mahowald, N., Milly, G., Faluvegi, G., Balkanski, Y., Collins, W. J., Conley, A. J., Dalsoren, S., Easter, R., Ghan, S.,

Horowitz, L., Liu, X., Myhre, G., Nagashima, T., Naik, V., Rumbold, S. T., Skeie, R., Sudo, K., Szopa, S., Takemura, T., Voulgarakis, A., Yoon, J.-H., and Lo, F.: Radiative forcing in the ACCMIP historical and future climate simulations, Atmos. Chem. Phys., 13(6), 2939-2974, 2013.

Streets, D. G., Bond, T. C., Carmichael, G. R., Fernandes, S. D., Fu, Q., He, D., Klimont, Z., Nelson, S. M., Tsai, N. Y., Wang, M. Q., Woo, J.-H., and Yarber, K. F.: An inventory of gaseous and primary aerosol emissions in Asia in the year 2000, J. Geophys. Res., 108, 8809, doi:10.1029/2002JD003093, 2003.

Streets, D. G., Yu, C., Wu, Y., Chin, M., Zhao, Z., Hayasaka, T., and Shi, G.: Aerosol trends over China, 1980–2000, Atmos. Res., 88(2): 174-182, 2008.

Taylor, K.E., Stouffer, R.J., and Meehl, G.A.: An Overview of CMIP5 and the experiment design, B. Am. Meteorol. Soc., 93, 485-498, doi:10.1175/BAMS-D-11-00094.1, 2012.

Wang, F., An, J. L., Li, Y., Tang, Y. J., Lin, J., Qu, Y., Chen, Y., Zhang, B., and Zhai, J.: Impacts of uncertainty in AVOC emissions on the summer ROx budget and ozone production rate in the three most rapidly-developing economic growth regions of China, Adv. Atmos. Sci., 31(6), 1331-1342, 2014.

Wang G, Zhang R, Gomez M E, et al. :Persistent sulfate formation from London Fog to Chinese haze., Proceedings of the Nat. Acad. of Sci., 201616540, 2016.

Wang, H., Shi, G. Y., Zhang, X. Y., Gong, S. L., Tan, S. C., Chen, B., Che, H. Z., and Li T.: Mesoscale modeling study of the interactions between aerosols and PBL meteorology during a haze episode in China Jing-Jin-Ji and its near surrounding region—Part 2: Aerosols' radiative feedback effects, Atmos. Chem. Phys., 15, 3277–3287, 2015.

Wang, S., Streets, D. G., Zhang, Q., He, K., Chen, D., Kang, S., Lu, Z., and Wang, Y.: Satellite detection and model verification of NOx emissions from power plants in Northern China, Environ. Res. Lett., 5, 044007, doi:10.1088/1748-9326/5/4/044007, 2010.

Wang, S., Zhang, Q., Streets, D. G., He, K. B., Martin, R. V., Lamsal, L. N., Chen, D., Lei, Y., and Lu, Z.: Growth in NOx emissions from power plants in China: bottom-up estimates and satellite observations, Atmos. Chem. Phys., 12, 4429-4447, 2012.

Wang, Y., Zhang, Q, Q, He, K., Zhang, Q., and Chai, L.: Sulfate-nitrate-ammonium aerosols over China: response to 2000–2015 emission changes of sulfur dioxide, nitrogen oxides, and ammonia, Atmos. Chem. Phys., 13(5), 2635-2652, 2013.

Wang, Y., Zhang, Q., Jiang, J., Zhou, W., et al.: Enhanced sulfate formation during China's severe winter haze episode in January 2013 missing from current models. J. Geophys. Res., 119, 10,425-10,440, doi:10.1002/2013JD021426, 2014.

Wang, Y. S., Yao, L., Wang, L., Liu, Z., et al.: Mechanism for the formation of the January 2013 heavy haze pollution episode over central and eastern China." Science China-Earth Sciences, 57(1): 14-25, 2014.

Xia, X., Chen, H., Goloub, P., Zhang, W., Chatenet, B., and Wang, P.: A complicaiton of aerosol optical properties and calculation of direct radiative forcing over an urban region in northern China, J. Geophy. Res., 112, d12203, doi:10.1029/2006JD008119, 2007a.

Xia, X., Chen, H., Li, Z., Wang, P., and Wang J.: Significant reduction of surface solar irradiance induced by aerosols in a suburban region in northeastern China, J. Geophys. Res., 112, doi:10.1029/2006JD007562, 2007b.

Xia, X., Li, Z., Holben, B., Wang, P., Eck, T., Chen, H., Cribb, M., and Zhao, Y.: Aerosol optical properties and radiative effects in the Yangtze Delta region of China, J. Geophys. Res., 112, D22S12, 2007c.

Xin, J., Wang, Y., Li, Z., Wang, P., Hao, W., Nordgren, B. L., Wang, S., Liu, G., Wang, L., Wen, T., Sun, Y., and Hu, B.: Aerosol optical depth (AOD) and Ångström exponent of aerosols observed by the Chinese Sun Hazemeter Network from August 2004 to September 2005, J. Geophys. Res.-Atmos., 112, D05203, doi:10.1029/2006JD007075, 2007.

Xing, J., Zhang, Y., Wang, S., Liu, X., Cheng S., Zhang, Q., Chen, Y., Streets, D. G., Jang, C., Hao, J., Wang, W.: Modeling study on the air quality impacts from emission reductions and atypical meteorological conditions during the 2008 Beijing Olympics, Atmos. Environ., 45(10), 1786-1798, 2011.

Zhang, K., Wan, H., Liu, X., Ghan, S. J., Kooperman, G. J., Ma, P.-L., Rasch, P. J., Neubauer, D., and Lohmann U.: Technical Note: On the use of nudging for aerosol–climate model intercomparison studies, Atmos. Chem. Phys., 14(16), 8631-8645, 2014.

Zhang, L., Henze, D. K., Grell, G. A., Carmichael, G. R., Bousserez, N., Zhang, Q., Torres, O., Ahn, C., Lu, Z., Cao, J., and Mao, Y.: Constraining black carbon aerosol over Asia using OMI aerosol absorption optical depth and the adjoint of GEOS-Chem, Atmos. Chem. Phys., 15, 10281–10308, 2015.

Zhang, L., Jacob, D. J., Boersma, K. F., Jaffe, D. A., Olson, J. R., Bowman, K. W., Worden, J. R., Thompson, A. M., Avery, M. A., Cohen, R. C., Dibb, J. E., Flock, F. M., Fuelberg, H. E., Huey, L. G., McMillan, W. W., Singh, H. B., and Weinheimer, A. J.: Transpacific transport of ozone pollution and the effect of recent Asian emission increases on air quality in North America: an integrated analysis using satellite, aircraft, ozonesonde, and surface observations, Atmos. Chem. Phys., 8, 6117–6136, 2008.

Zhang, Q., Streets, D. G., Carmichael, G. R., He, K. B., Huo, H., Kannari, A., Klimont, Z., Park, I. S., Reddy, S., Fu, J. S., Chen, D., Duan, L., Lei, Y., Wang, L. T., and Yao, Z. L.: Asian emissions in 2006 for the NASA INTEX-B mission, Atmos. Chem. Phys., 9, 5131–5153, 2009.

Zhang, Q., Geng, G. N., Wang, S. W., Richter, A., and He, K. B.: Satellite remote sensing of changes in NOx emissions over China during 1996-2010, Chin. Sci. Bull., 57, 2857-2864, 2012.

Zhang, R., Jing, J., Tao, J., Hsu, S.-C., Wang, G., Cao, J., Lee, C. S. L., Zhu, L., Chen, Z., Zhao, Y., and Shen, Z.: Chemical characterization and source apportionment of PM2.5 in Beijing: seasonal perspective, Atmos. Chem. Phys., 13(14), 7053-7074, 2013.

Zhao, P. S., Dong, F., He, D., Zhao, X. J., Zhang, X. L., Zhang, W. Z., Yao, Q., and Liu, H. Y.: Characteristics of concentrations and chemical compositions for PM2.5 in the region of Beijing, Tianjin, and Hebei, China, Atmos. Chem. Phys., 13, 4631-4644, 2013.

Zhao, Y., Nielsen, C.P., Lei, Y., McElroy, M.B., Hao, J.: Quantifying the uncertainties of a bottom-up emission inventory of anthropogenic atmospheric pollutants in China, Atmos. Chem. Phys., 11, 2295–2308, 2011.

Zheng, B., Zhang, Q., Zhang, Y., He, K. and et al.: Heterogeneous chemistry: a mechanism missing in current models to explain secondary inorganic aerosol formation during the January 2013 haze episode in North China. Atmos. Chem. Phys., 15, 2031-2049, doi:10.5194/acp-15-2031-2015, 2015.

Zhuang, B.L., Wang, T.J., Li, S., Liu, J., Talbot, R., Mao, H.T., Yang, X.Q., Fu, C.B., Yin, C.Q., Zhu, J. L., Che, H.Z., and Zhang, X.Y.: Optical properties and radiative forcing of urban aerosols in Nanjing, China, Atmos. Environ., 83, 43-52, 2014.

Table 1. AOD averaged over eastern China in 2009 simulated using the MEIC and the AR5 emissions.

Species	MEIC AOD	AR5 AOD	(MEIC-AR5)/AR5 AOD	(MEIC-AR5)/AR5 Emission
Sulfate	0.085	0.059	44.29%	12.57%
BC	0.030	0.021	42.58%	13.35%
POM	0.044	0.026	70.35%	12.04%
SOA	0.031	0.026	17.40%	46.88%
Dust	0.057	0.056	1.00%	0.00%
Sea salt	0.006	0.005	4.24%	0.00%
All aerosols	0.252	0.193	30.38%	-

760

Table 2. Aerosol direct radiative effects (ADRE) and the normalized radiative effect (NRE) averaged over eastern China in 2009 simulated using the MEIC and the AR5 emissions.

	Species	MEIC ADRE, Wm^{-2}	AR5 ADRE, Wm^{-2}	(MEIC-AR5)/AR5 ADRE, %	MEIC NRE, Wm^{-2} τ_{aer}^{-1}	AR5 NRE, Wm^{-2} τ_{aer}^{-1}	*Schulz et al.*, [2006] NRE, Wm^{-2} τ_{aer}^{-1}
TOA	All aerosols	-0.50	-0.31	63.32%	-2.62	-2.71	
	Sulfate	-1.03	-0.75	36.88%	-14.34	-15.29	-19 (-32 to -10)
	BC	2.92	2.25	29.91%	122.40	122.79	153 (28 to 270)
	POM	-0.59	-0.35	66.03%	-14.71	-16.02	-19 (-38 to -5)
Surface	All aerosols	-12.76	-10.34	23.42%	-50.49	-53.11	
	Sulfate	-1.69	-1.27	33.01%	-21.87	-23.83	
	BC	-4.45	-3.34	33.35%	-158.82	-163.35	
	POM	-1.81	-1.12	60.94%	-42.16	-44.64	
Atmosphere	All aerosols	12.26	10.03	22.20%	47.87	50.40	
	Sulfate	0.66	0.52	27.40%	7.53	8.54	
	BC	7.38	5.59	31.96%	281.22	286.13	
	POM	1.22	0.77	58.59%	27.45	28.63	

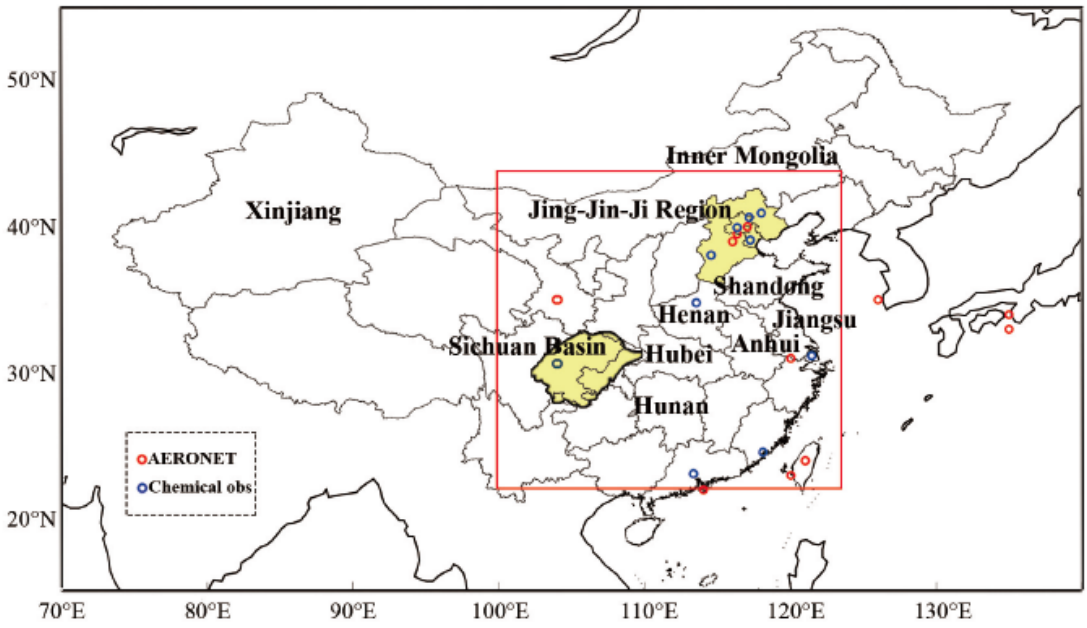

765

Figure 1. Geographical locations of the AERONET sites and chemical composition sites where the observational data are used in this study. The provinces and regions mentioned in the context are marked. The red frame denotes eastern China (22-44^{o} N, 100-124^{o} E).

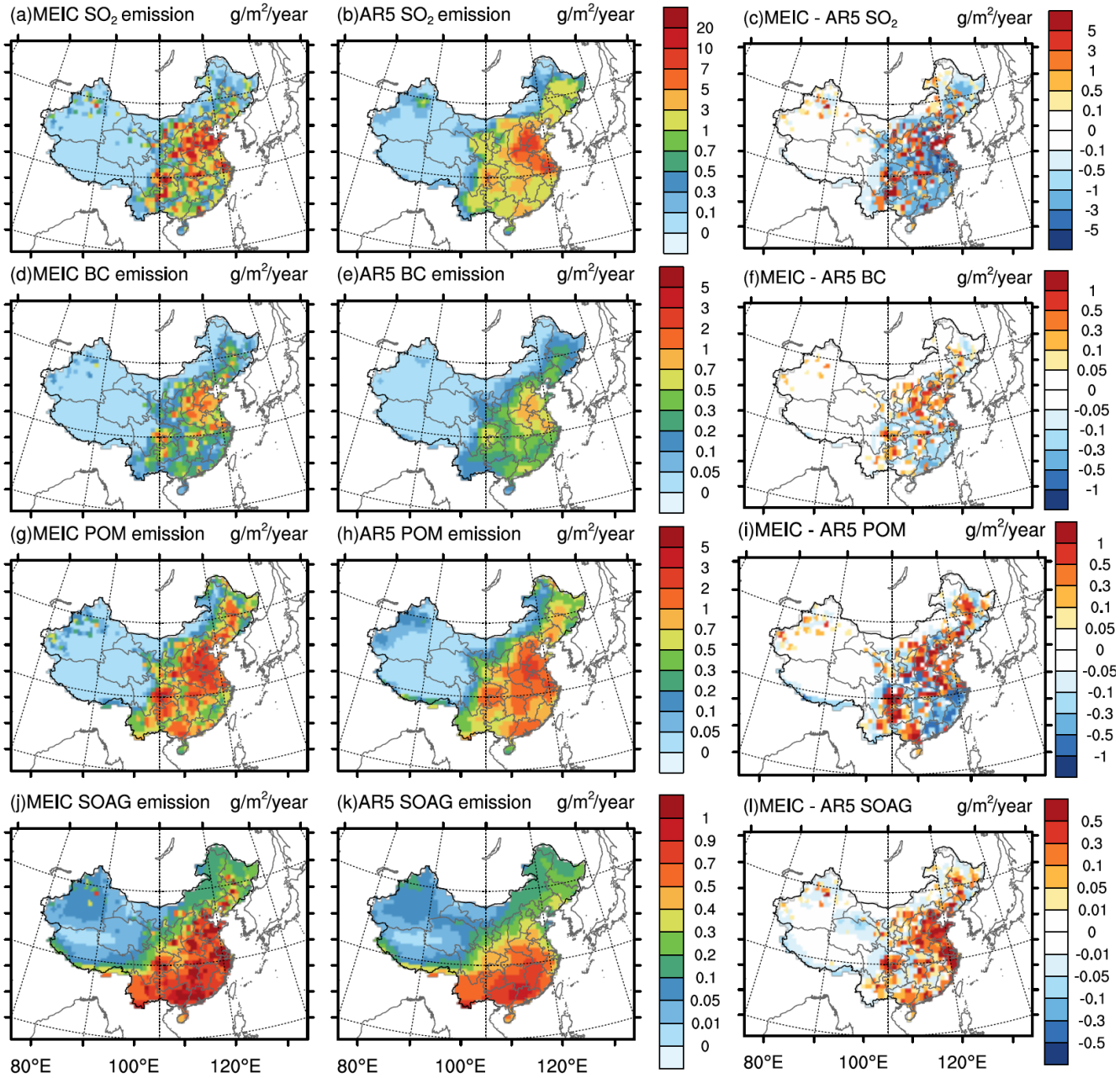

Figure 2. The spatial distributions of the MEIC emission, the AR5 emission and their difference for (a)-(c) SO_2, (d)-(f) BC, (g)-(i) POM, and (j)-(l) SOAG of year 2009 in China.

775

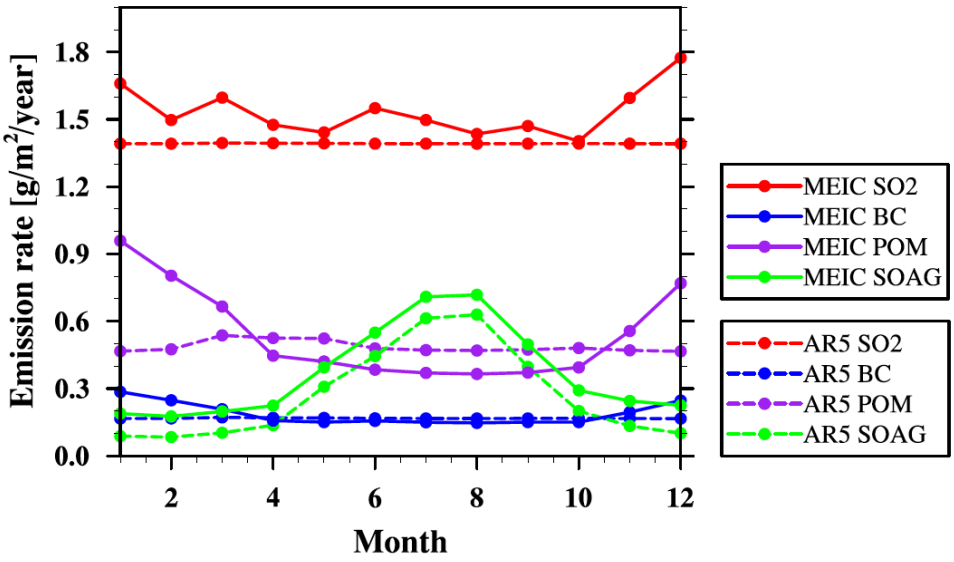

Figure 3. Seasonal variation of sulfate, BC, POM, and SOAG in the MEIC emission and the AR5 emission in eastern China.

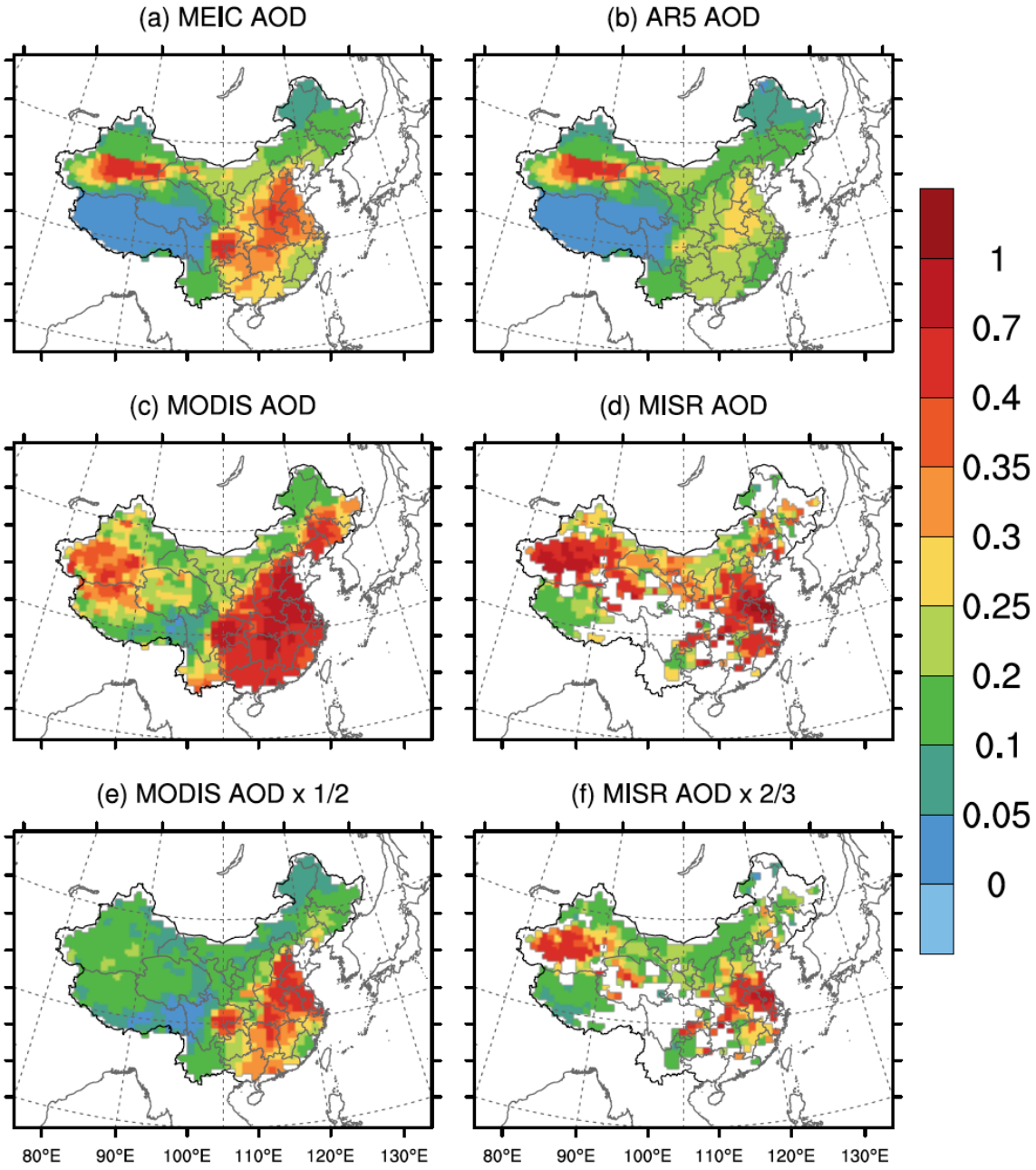

Figure 4. Spatial distributions of annual averaged AOD at 550 nm over China in 2009 simulated by CAM5-MAM3 using (a) the MEIC emission, (b) the AR5 emission, observed by (c) MODIS and (d) MISR satellites, (e) One-half of the AOD observed by MODIS, and (f) two thirds of the AOD observed by MISR.

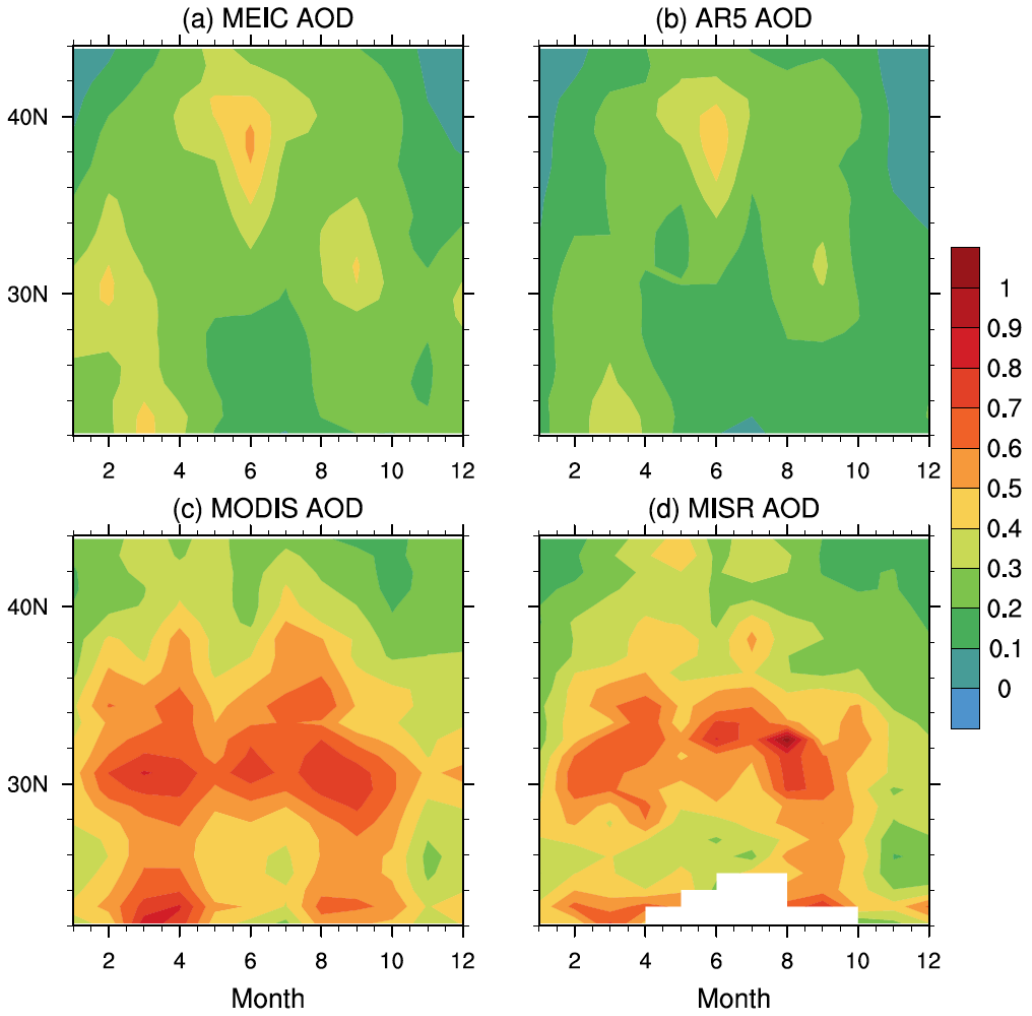

Figure 5. The seasonal variation of longitudinal averaged (100° E-124° E) AOD at 550 nm over eastern China simulated by CAM5-MAM3 using (a) the MEIC emission, (b) the AR5 emission, observed by (c) MODIS, and (d) MISR satellites in 2009.

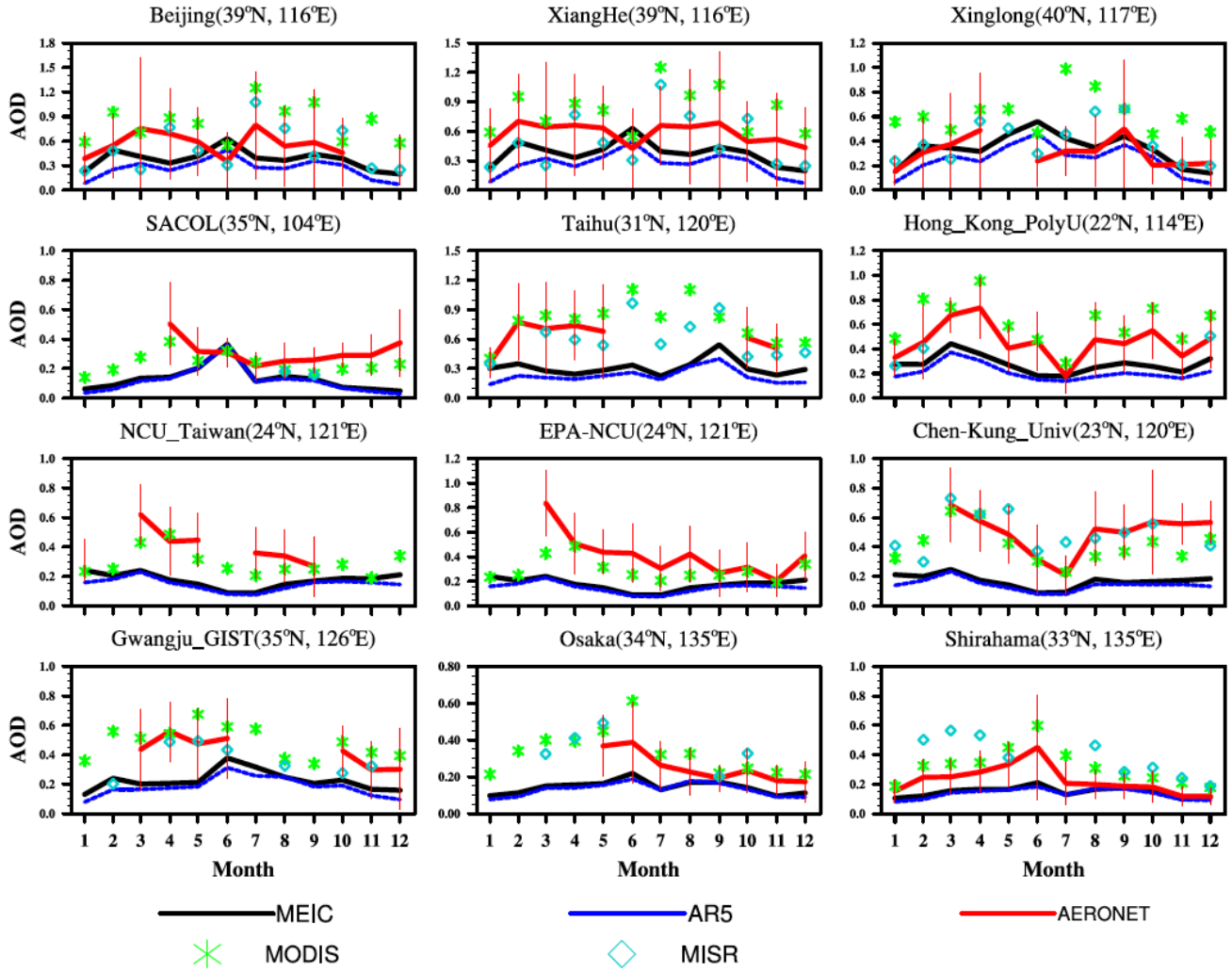

Figure 6. Monthly averaged AOD simulated by CAM5-MAM3 using the MEIC emission and the AR5 emission compared with the AERONET, MODIS and MISR observations at 12 locations in and around China. The error bars represent one standard deviation of the daily AERONET observations within the month.

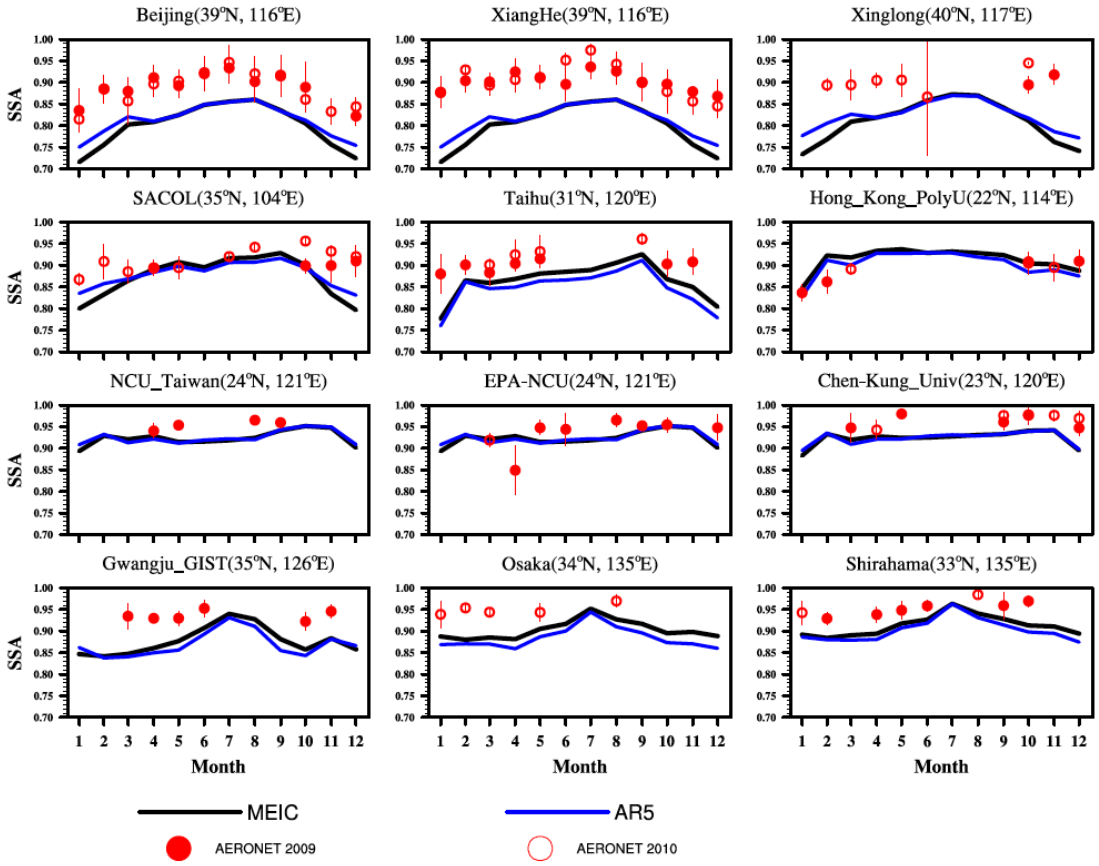

Figure 7. The seasonal variation of SSAs simulated by CAM5-MAM3 using the MEIC emission and the AR5 emission and observed by AERONET (red dots) at 12 AERONET sites in and around China. Error bars stand for one standard deviations of the observations.

800

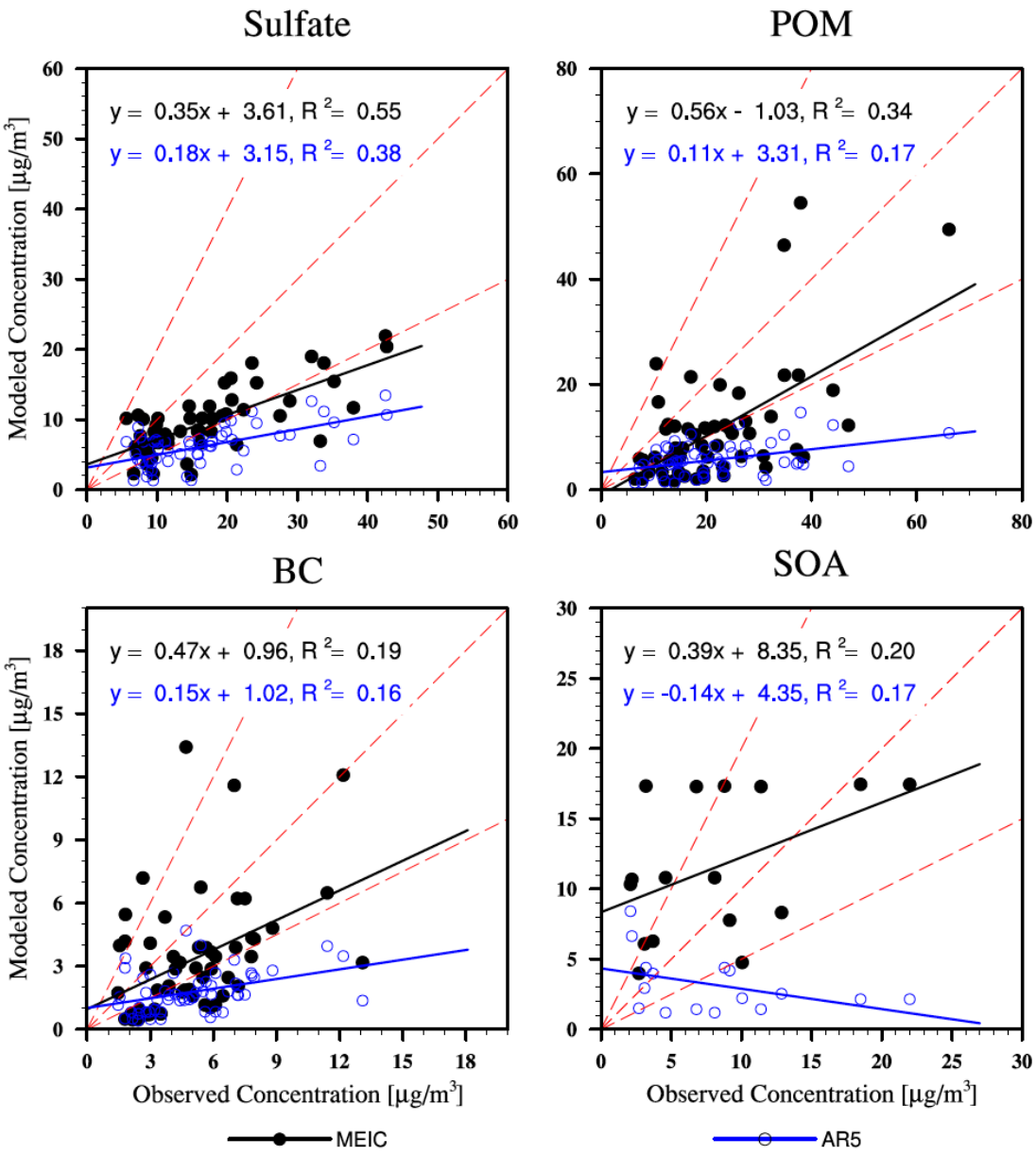

Figure 8. The monthly averaged surface concentrations of sulfate, POM, BC, and SOA using the MEIC emission and the AR5 emission compared with observations. The solid lines are linear regressions between the model results and observations. The red dashed lines represents the 1:2, 1:1, and 2:1 lines. The regression functions and the correlation coefficients (R^2) are also shown.

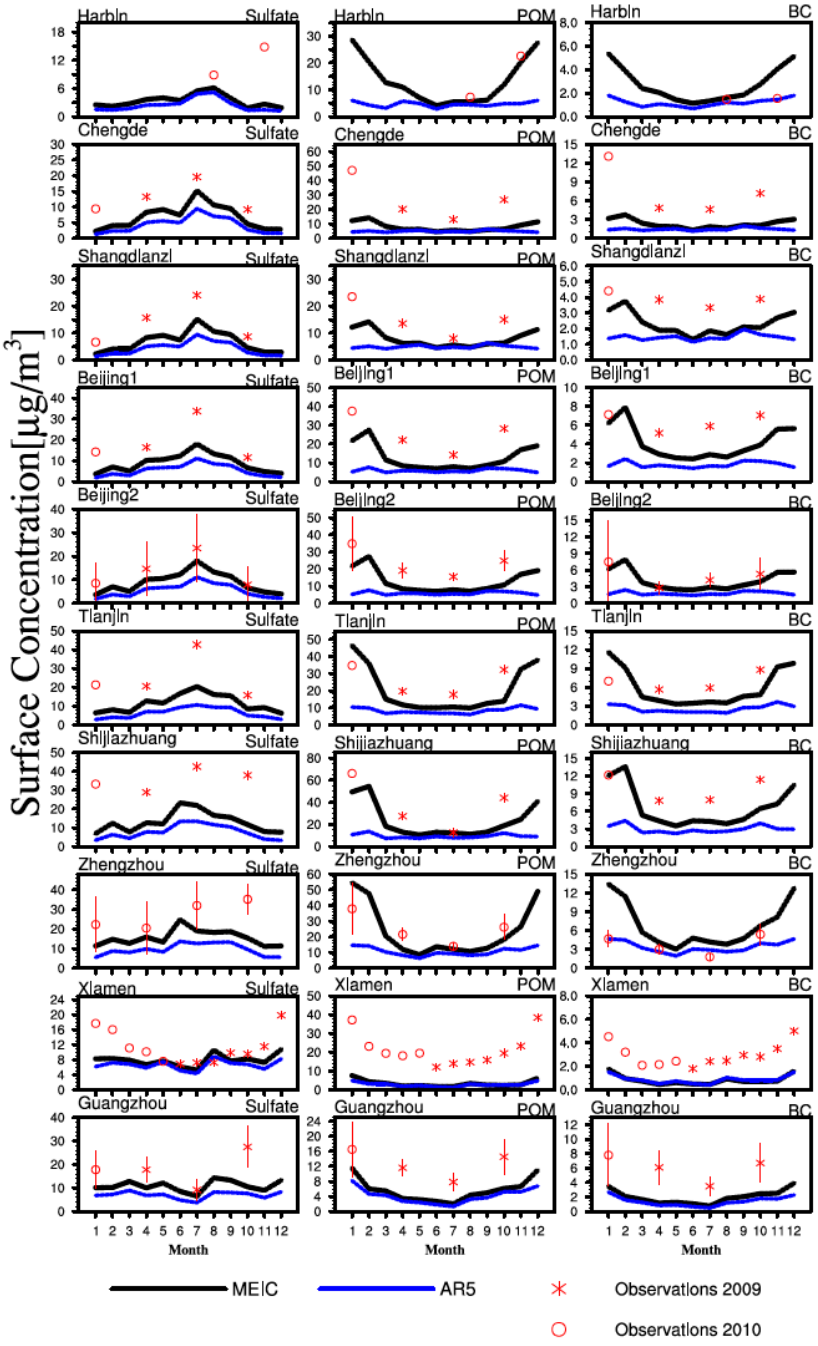

805

Figure 9. The seasonal variation of monthly averaged surface concentrations of sulfate, POM, and BC modeled by CAM5-MAM3 using MEIC and AR5 emissions compared with the observations. Error bars stand for one standard deviation

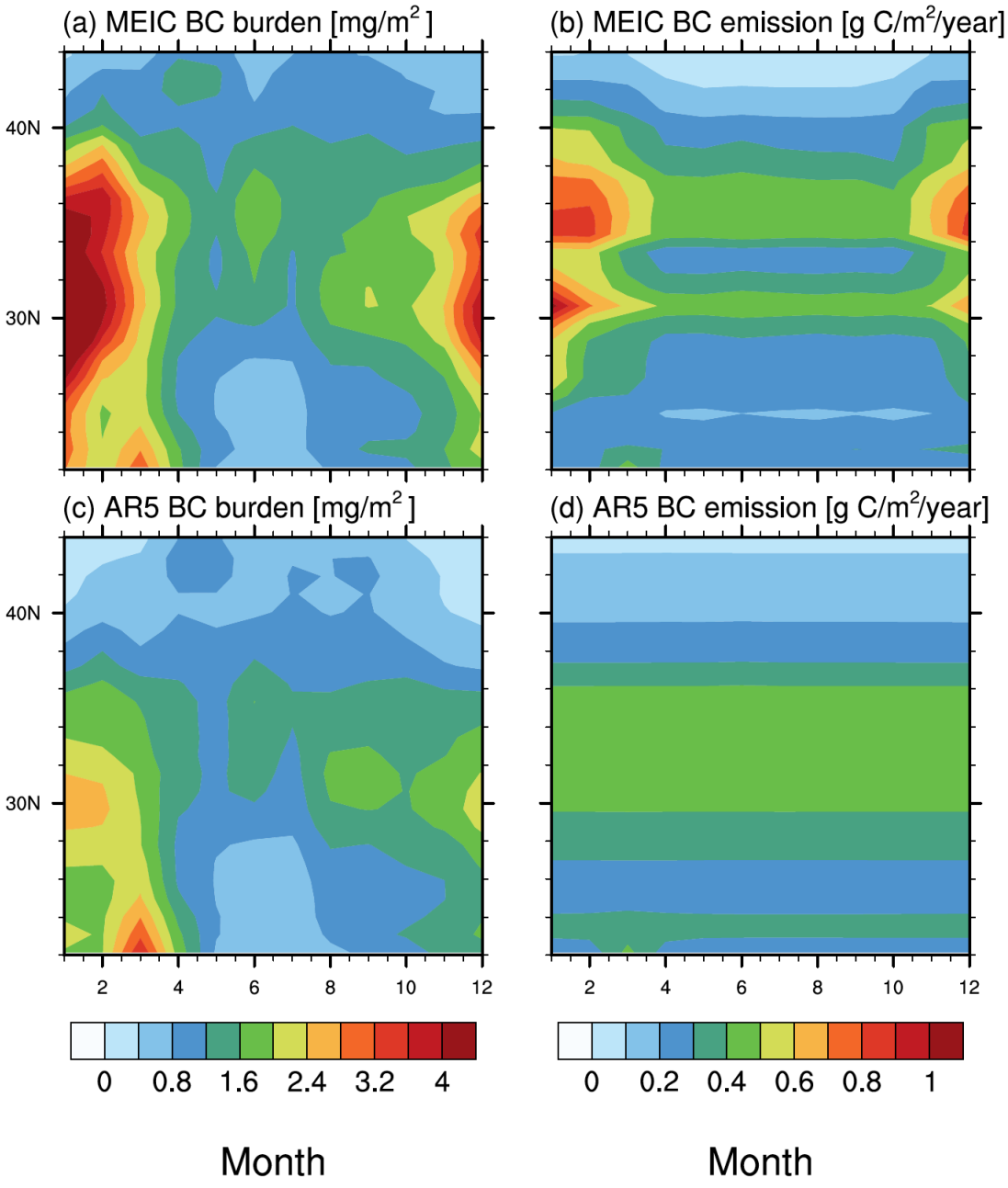

Figure 10. The seasonal variation of longitudinal averaged (100° E-124° E) of (a) burden of BC, (b) emission rate of BC using the MEIC emission, (c) burden of BC, (d) emission rate of BC using the AR5 emission inventory over eastern China in 2009.

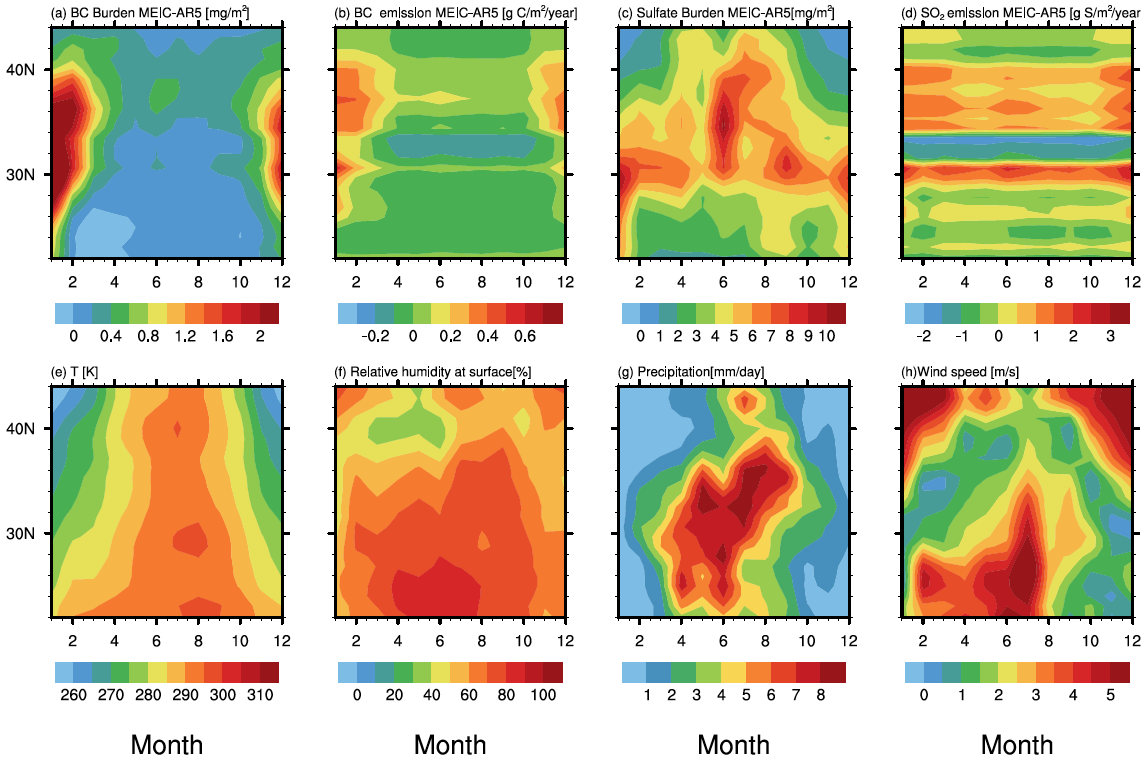

Figure 11. The seasonal variation of longitudinal averaged (100° E-124° E) differences of (a) BC burden, (b) BC emission, (c) sulfate aerosol burden, and (d) SO_2 emission from the MEIC emission and the AR5 emission runs with identical meteorological variables of (e) temperature, (f) relative humidity at surface, (g) precipitation, and (h) horizontal wind speed over eastern China in 2009.

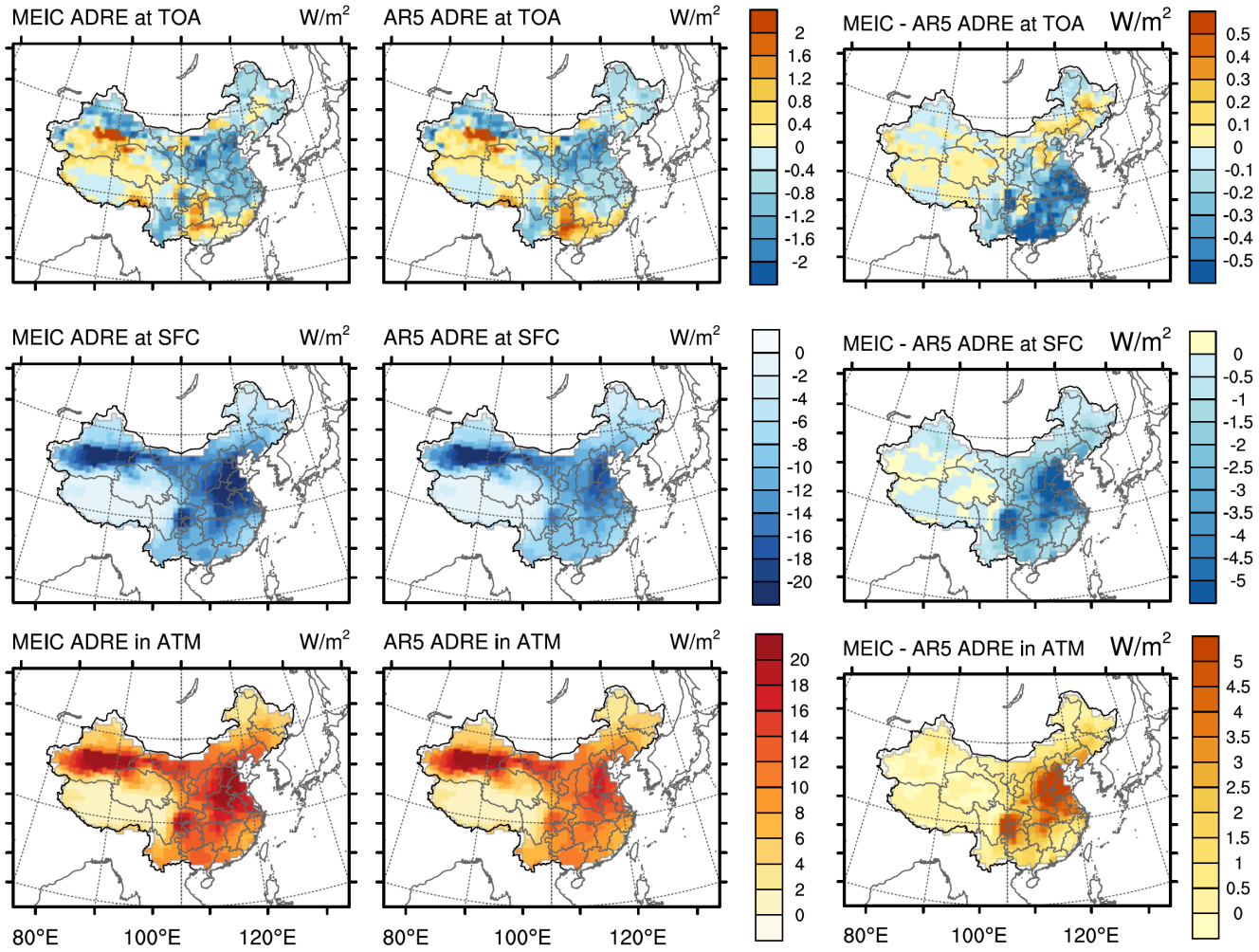

Figure 12. Spatial distributions of the annual averanged aerosol direct radiative effects (ADREs) at TOA, surface (SFC) and in the atmosphere (ATM) using the MEIC and the AR5 emissions and their differences.

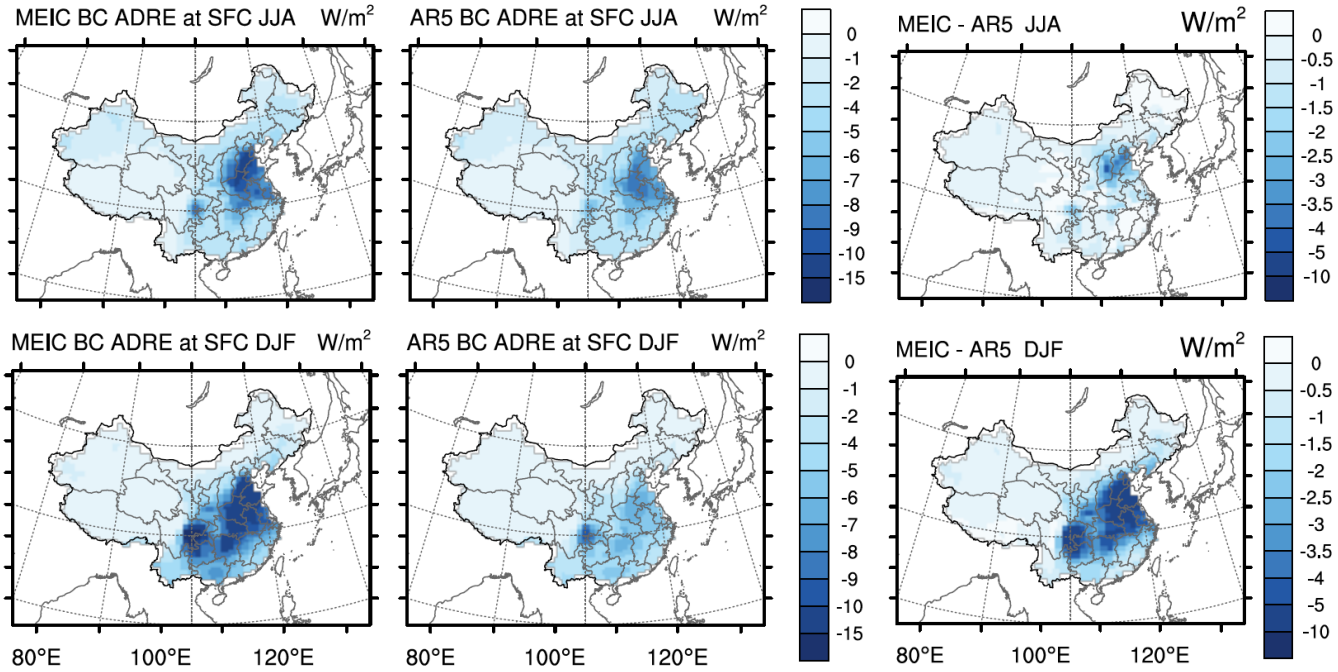

Figure 13. Spatial distributions of ADREs of BC in the summer (June, July, August) and the winter (December, January, February) at the surface (SFC).

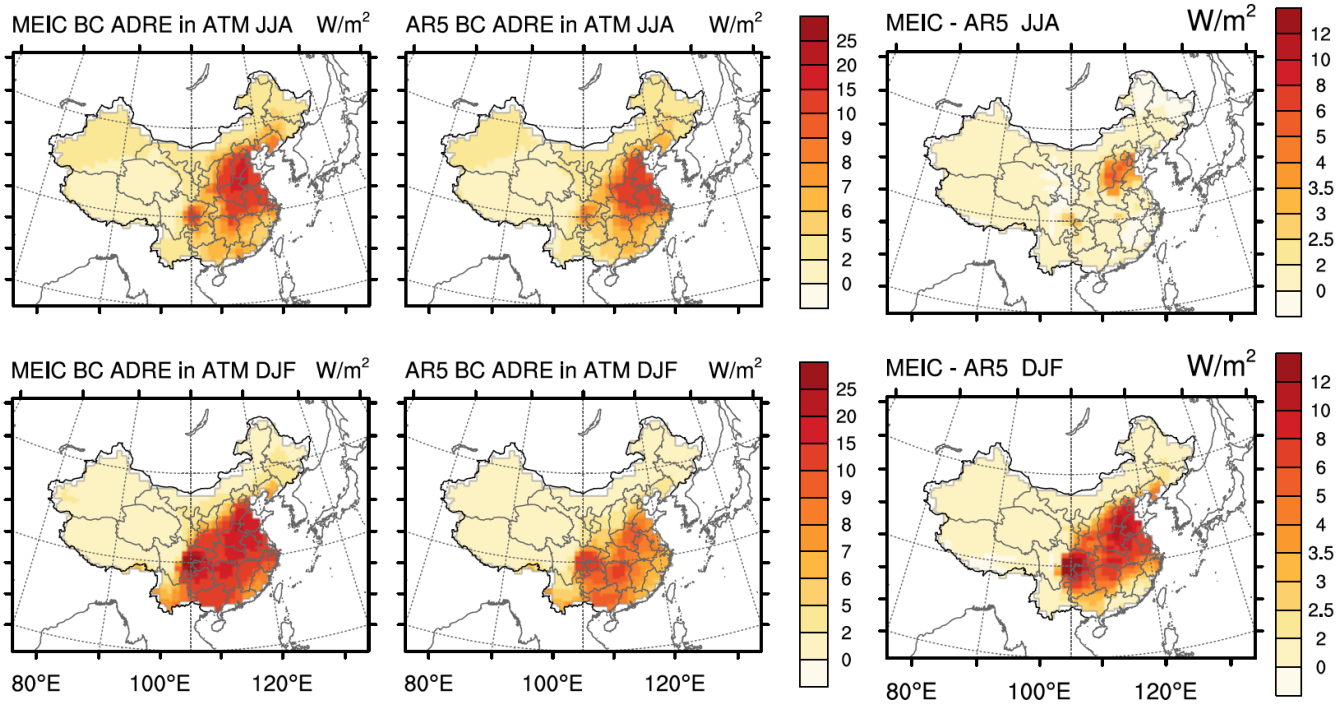

Figure 14. Same as Figure 13 but for the ADRES of BC in the atmosphere (ATM).

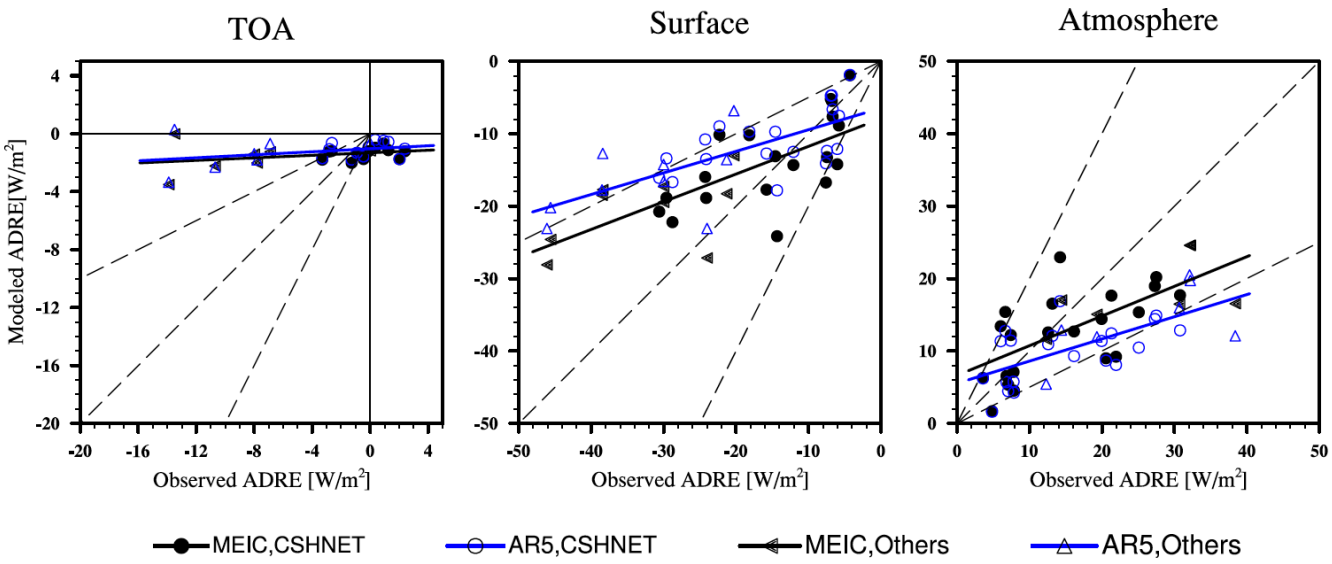

Figure 15. ADREs at TOA, surface, and atmosphere modeled by CAM5-MAM3 using the MEIC and the AR5 emissions compared with ADRE observations in China.

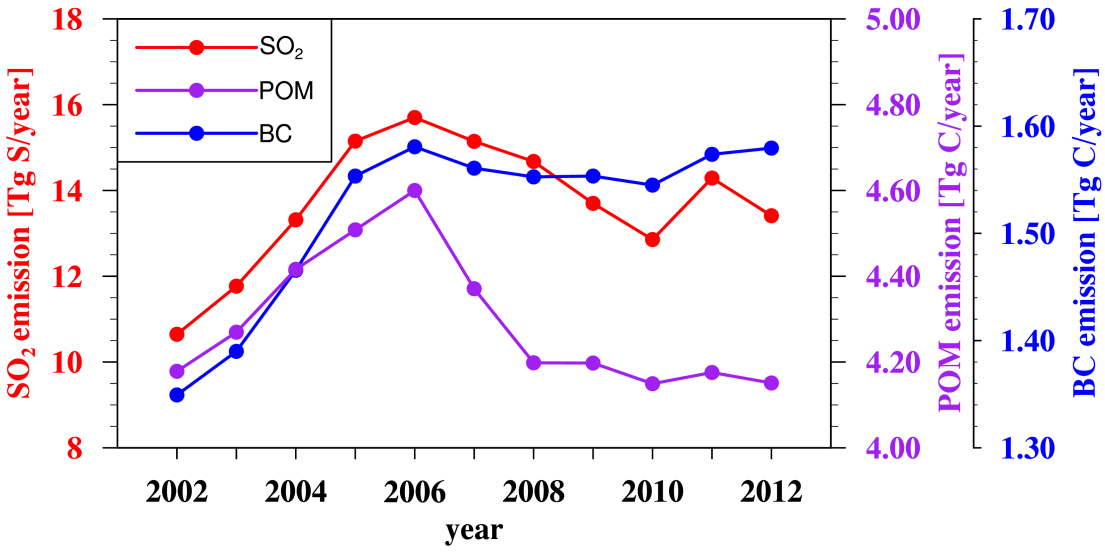

Figure 16. The change of emission rates of SO_2, BC, and POM from year 2002 to 2012 in eastern China.

845

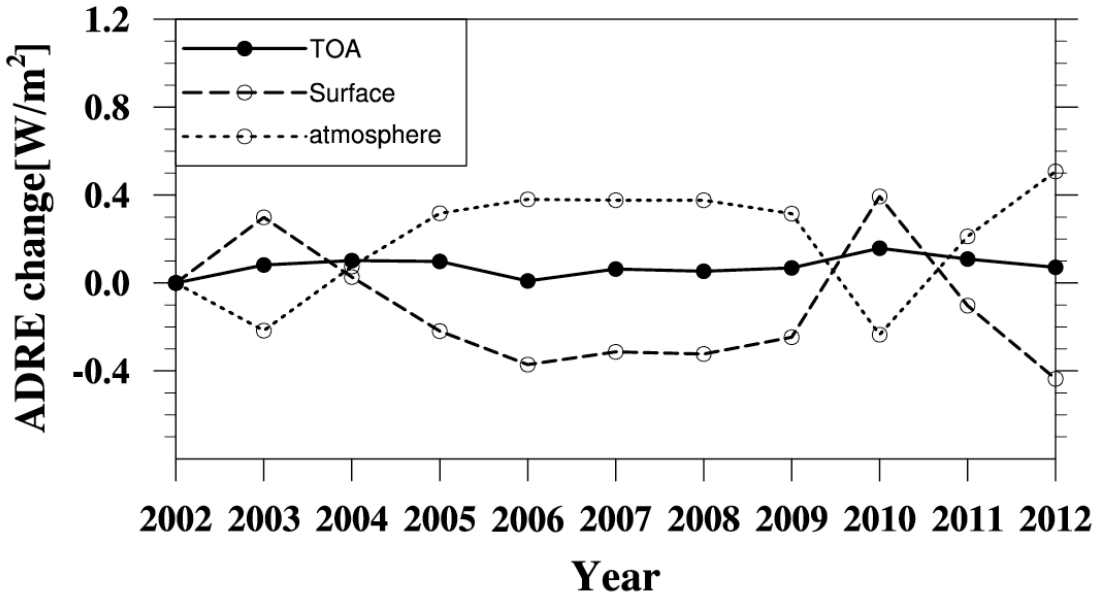

Figure 17. The change of ADREs at TOA, surface and in the atmosphere relative to year 2002 with MEIC emission in eastern China.